

Chapter 32: Reaction Dynamics

Calculate the bimolecular rate constant of the reaction $\text{H}_2(\text{g}) + \text{F}_2(\text{g}) \rightarrow 2 \text{HF}(\text{g})$ at 298.2 K. The experimental activation energy is 50.0 kJ mol^{-1} .

The extent of a chemical reaction is determined by thermodynamics. The rate of a chemical reaction is determined by chemical kinetics. Molecules must collide for a chemical reaction to occur. The sequence of elementary steps, as specified by the collision partners, determine the mechanism. The rate constants of elementary steps are calculated using **reaction dynamics**. Kinetic molecular theory provides a good estimate of the rate of collisions of ideal gases. However, not all collisions are successful in producing products. The key to understanding bond rearrangements during collisions is the postulation of the transition state. The bond breaking and making steps can be understood in coarse-grained detail by assuming the statistical distribution of the available energy among the degrees of freedom of the transition state. This statistical mechanical view is the basis of activated complex theory and thermodynamic transition state theory. In fine-grained detail, collision dynamics follows the flow of energy in the transition state assuming a quantum mechanical potential energy surface. In the laboratory, molecular beam techniques provide the experimental information necessary to validate reaction dynamics theories. The results of experimental studies are also used to extend kinetic molecular theory to better understand collision kinematics, taking molecular interactions into account. Reaction dynamics in solution is based on gas-phase dynamics utilizing the concept of a molecular encounter instead of discrete collisions.

Accurate reaction dynamics theories of complex mechanistic steps are an important goal with far reaching implications. Reaction dynamics is currently a highly active area of research in physical chemistry. The passage of a collision through the transition state is the principle focus of our prediction of rate constants.

32.1 The Transition State

The Reaction Coordinate is an Unstable Asymmetric Stretch: Consider the gas phase atom-diatom reaction:



Before the collision the HF molecule is in a vibrational potential energy well centered on the equilibrium internuclear separation $R_e(\text{HF})$, giving a “bound” vibration, Figure 32.1.1a. After the reaction the H_2 molecule is in an analogous vibrational potential energy well centered on the equilibrium internuclear separation $R_e(\text{H}_2)$, giving a bound vibration. The vibrations are each characterized by a corresponding fundamental vibration frequency $\nu_0 = 1/2\pi \sqrt{k/\mu}$. During the collision, the H-atom approaches the H-F molecule. The progress of the reaction occurs on the reaction profile, Figure 32.1.1b. The reaction profile is a plot of the minimum electronic energy path from reactants to products. The reaction path follows the profile energy with the addition of the zero-point energy of the corresponding vibrations. The **transition state** occurs when the H–H distance is roughly equal to the H–F distance, when the H–H bond forms simultaneously as the H–F bond breaks. The transition state occurs at the energy maximum of the reaction profile. The transition state lasts for a fleeting instant in time, typically on the order of a few femtoseconds. The motion of the three atoms during the collision shows the same atom displacements as the

asymmetric stretch of a linear triatomic, Figures 27.1.3 and 8.11.1. This **reactive asymmetric stretch** is the reaction coordinate. However, the motion during the collision corresponds to a maximum in the reaction profile, making the reactive asymmetric stretch unstable. The transition state corresponds to a surface, perpendicular to the reaction coordinate, separating the products from the reactants. A successful reaction corresponds to passage across this surface. For the H + HF example, a successful collision progresses to products giving an H₂ molecule in a bound vibrational state and a free F-atom. An unsuccessful collision falls apart returning to reactants.

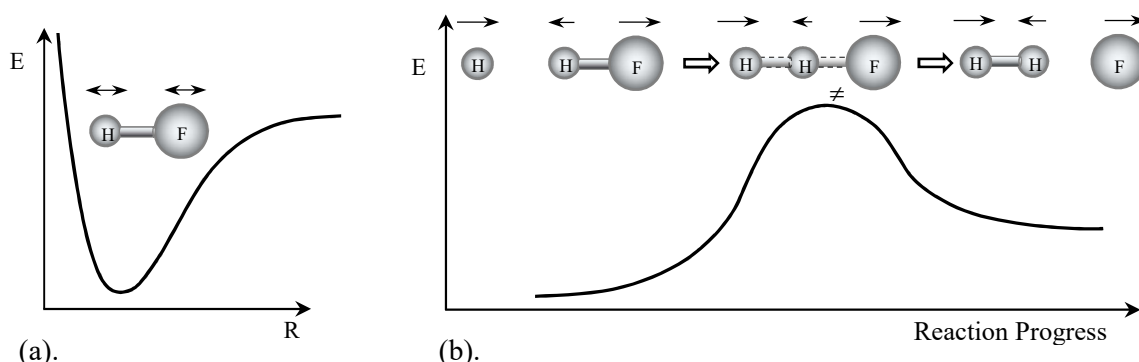


Figure 32.1.1: (a). A bound vibration results from a potential energy minimum. (b). The reaction coordinate is the progress along the reactive asymmetric stretch. The reaction profile has a maximum in potential energy at the transition state.

The Rate is Determined by the Frequency of the Reactive Asymmetric Stretch: The reaction progress is plotted as the horizontal axes of the reaction profile and corresponds to the progress of the reactive asymmetric stretch. The configuration of atoms at the transition state is called the **activated complex**. Properties of the activated complex are symbolized using “≠.” The “activated” part indicates that sufficient energy is available to bring about the bond breaking and making steps. The energy is supplied by the relative translational kinetic energy of the collision and possibly the initial vibrational and rotational energies of the reactants. The term “complex” however, can be misleading. While some activated complexes exist for a few vibrational periods of the reactive asymmetric stretch, the transition state is not a complex at all. Rather, the activated complex is a “loose and floppy” transitory intermediate that typically falls forwards towards products or backwards towards reactants within a single vibrational period. The effective vibrational frequency of the reactive asymmetric stretch, ν^\ddagger , is the frequency at which the activated complex crosses the transition state surface. As a first approximation, the activated complex falls apart forwards towards products half the time with rate ν^\ddagger and backwards towards reactants half the time with rate ν^\ddagger .

Consider now a general reaction, where reactants A and B are atoms or molecules. The reactive asymmetric stretch carries the reaction towards the transition state and the formation of the activated complex, AB[‡]:



The classical rate law for a bimolecular mechanistic step has the form:

$$-\frac{d[A]}{dt} = k_2 [A][B] \quad 32.1.3$$

Activated complex theory, ACT, expresses the reaction rate as the product of the concentration of the activated complex and the vibrational frequency of the reactive asymmetric stretch:

$$-\frac{d[A]}{dt} = \nu^\ddagger [AB^\ddagger] \quad 32.1.4$$

Comparing the classical and ACT expressions, Eqs. 32.1.3 and 32.1.4, the bimolecular rate constant is given as:

$$k_2 = \frac{\nu^\ddagger [AB^\ddagger]}{[A][B]} \quad 32.1.5$$

The concentration of the activated complex can be considered to be in equilibrium with the reactants, with equilibrium constant K_c^\ddagger :

$$K_c^\ddagger = \frac{[AB^\ddagger]}{[A][B]} \quad \text{giving} \quad k_2 = \nu^\ddagger K_c^\ddagger \quad 32.1.6^\circ$$

In this expression K_c^\ddagger has units of $L \text{ mol}^{-1}$. The assumption of equilibrium is not necessary, however the assumption simplifies the mathematics of the derivation.

Partition Functions Determine the Number of Accessible States in the Activated Complex:

Statistical mechanics provides useful insight into equilibrium constants of chemical reactions. The statistical mechanical approach assumes the available thermal kinetic energy is distributed according to the Boltzmann distribution, which is applied to each degree of freedom of the activated complex: translational, rotational, and vibrational. However, the statistical mechanical expression for the equilibrium constant is for K_p , whereas the kinetic expressions are typically written in terms of concentrations. K_p and K_c , with concentration units, are related by Eq. 20.2.5:

$$K_p = K_c \left(\frac{RT}{P^\circ} \right)^{\Delta n_g} \quad K_c \text{ with units } (\text{mol L}^{-1})^{\Delta n_g} \quad (20.2.5) \quad 32.1.7^\circ$$

where Δn_g is the change in number of moles of gas and P° is the standard state pressure. For the formation of the transition state, $A + B \rightarrow AB^\ddagger$, the change in number of moles is -1 . The concentration based equilibrium constant of the formation of the activated complex is then:

$$K_c^\ddagger = K_p^\ddagger \left(\frac{RT}{P^\circ} \right) \quad \text{giving} \quad k_2 = \nu^\ddagger \left(\frac{RT}{P^\circ} \right) K_p^\ddagger \quad 32.1.8^\circ$$

Each degree of freedom is assumed to be at equilibrium with the available thermal energy, which is distributed according to random statistical chance giving the most probable state. The equilibrium constant is the number of accessible states of the activated complex divided by the number of accessible states of the reactants. Using Eq. 30.5.18°:

$$K_c^\ddagger = \frac{[AB^\ddagger]}{[A][B]} = \frac{q^{\ddagger^\circ}/N_A}{(q_A^\circ/N_A)(q_B^\circ/N_A)} \left(\frac{RT}{P^\circ} \right) e^{-\Delta E_0^\ddagger/kT} \quad 32.1.9^\circ$$

where q^{\ddagger° , q_A° , and q_B° are the standard state partition functions of the activated complex, reactant A, and reactant B, respectively. The energy parameter that characterizes the transition state is

the quantum mechanical zero-point energy shift, ΔE_0^\ddagger , Figure 32.1.2 (compare with Figure 30.5.1). The activation energy and ΔE_0^\ddagger are distinct but closely related, see below. At the level of approximation of ACT, the energies along the reaction profile are determined using the Born-Oppenheimer approximation.

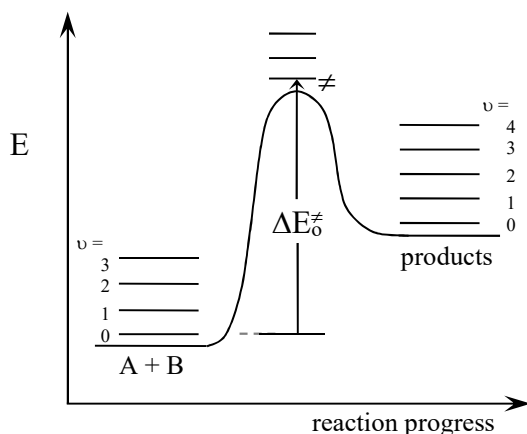


Figure 32.1.2: The reaction progress is the progress of the reactive asymmetric stretch. The energy axis is E = total electronic + rotation + vibration without the reactive asymmetric stretch. The transition state barrier is the quantum mechanical zero-point energy shift, ΔE_0^\ddagger . The shorter horizontal lines represent vibrational states, other than the reactive asymmetric stretch. Rotational states are not shown.

The partition function of the activated complex includes all normal modes of the activated complex. However, one of the normal modes is the reactive asymmetric stretch. The overall partition function of the activated complex is the product of the partition function of the reactive asymmetric stretch, q_v^\ddagger , and the partition function of the remaining translational, rotational, vibrational, and electronic degrees of freedom, $q^{\neq o'}$:

$$q^\ddagger = q_v^\ddagger q^{\neq o'} \quad 32.1.10^\circ$$

The vibrational partition function of the reactive asymmetric stretch is, Eq. 30.2.25:

$$q_v^\ddagger = \frac{1}{(1 - e^{-h\nu^\ddagger/kT})} \quad 32.1.11^\circ$$

The frequency of the reactive asymmetric stretch is quite small, given that the activated complex is loosely bond and unstable. Assuming that $h\nu^\ddagger/kT \ll 1$, the Boltzmann weighting factors can be expanded as a power series. Retaining only the first two terms, the partition function is given in the high temperature approximation as, Eq. 30.4.20:

$$e^{-h\nu^\ddagger/kT} = 1 - h\nu^\ddagger/kT + \dots \quad \text{giving} \quad q_v^\ddagger = \frac{kT}{h\nu^\ddagger} \quad 32.1.12^\circ$$

Substituting this result into Eq. 32.1.10^o gives the partition function of the activated complex as:

$$q^\ddagger = \frac{kT}{h\nu^\ddagger} q^{\ddagger\circ'} \quad \text{and} \quad K_c^\ddagger = \frac{kT}{h\nu^\ddagger} K_c^{\ddagger\prime} \quad 32.1.13^\circ$$

where $K_c^{\ddagger\prime}$ is the equilibrium constant without the reactive asymmetric stretch. Substitution of K_c^\ddagger into Eq. 32.1.6 $^\circ$ and the activated complex partition function into Eq. 32.1.9 $^\circ$ gives the bimolecular rate constant as:

$$k_2 = \frac{kT}{h} K_c^{\ddagger\prime} = \frac{kT}{h} \frac{q^{\ddagger\circ'}/N_A}{(q_A^\circ/N_A)(q_B^\circ/N_A)} \left(\frac{RT}{P^\circ}\right) e^{-\Delta E_0^\ddagger/kT} \quad 32.1.14^\circ$$

Even though the factors of ν^\ddagger cancel, the reactive asymmetric stretch is still represented through the kT/h factor. The kT/h factor represents the statistical distribution of available thermal kinetic energy into the reactive asymmetric stretch. The strength of ACT is that the relationship in Eq. 32.1.14 $^\circ$ is readily interpreted in terms of the number of accessible states of the activated complex and the reactants, as in Example 30.4.5. Activated complex theory presents a distinctly different view of chemical dynamics compared to hard-core collision theory. However, are ACT and hard-core collision theory to some extent consistent?

Atom-Recombination Under ACT is Consistent with Hard-Core Collision Theory: Hard-core collision theory represents collisions between spherical structureless particles. In the richer context of ACT, atom-recombination reactions mimic the hard-core collision theory assumptions. The general reaction is $A + B \rightarrow A \cdots B^\ddagger$, where A and B are atoms. Consider first the translational partition functions in Eq. 32.1.14 $^\circ$. The masses are m_A , m_B , and $m^\ddagger = m_A + m_B$. The reduced mass of the collision is $\mu = (m_A + m_B)/m^\ddagger$. The translational partition functions are given by Eq. 30.2.19 $^\circ$. The ratio of the partition functions is:

$$\frac{(q_t^{\ddagger\circ}/N_A)}{(q_t^\circ(A)/N_A)(q_t^\circ(B)/N_A)} = \frac{N_A h^3}{(2\pi kT)^{3/2} V_m^\circ} \left(\frac{m^\ddagger}{m_A m_B}\right)^{3/2} = \frac{N_A h^3}{(2\pi\mu kT)^{3/2} V_m^\circ} \quad 32.1.15^\circ$$

The rotational partition function of the activated complex is given by Eqs. 30.2.33, 24.5.41 and 24.4.10:

$$q_{r,i} = \frac{kT}{\sigma \tilde{B}_i hc} \quad \text{with} \quad \tilde{B}_i = \frac{h}{8\pi^2 \mu R_i^2 c} \quad \text{gives} \quad q_r^\ddagger = \left(\frac{8\pi^2 kT}{\sigma h^2}\right) \mu R^{\neq 2} \quad 32.1.16$$

where R^\neq is the bond length in the activated complex. If A and B are different atoms the symmetry number is $\sigma = 1$, while if A collides with A, the activated complex is symmetric and then $\sigma = 2$. The stretching vibration of the activated complex is the reaction coordinate, which is represented by the kT/h term. To mimic the structureless particles of hard-core collision theory, we assume that the electronic partition functions are unity. Also note that in Eq. 32.1.15 $^\circ$, $RT/P^\circ = V_m^\circ$. The overall bimolecular rate constant using Eq. 32.1.15 $^\circ$ is:

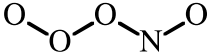
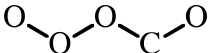
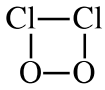
$$\begin{aligned} k_2 &= \frac{kT}{h} \frac{N_A h^3}{(2\pi\mu kT)^{3/2} V_m^\circ} \left(\frac{8\pi^2 kT}{\sigma h^2}\right) \mu R^{\neq 2} V_m^\circ e^{-\Delta E_0^\ddagger/kT} \\ &= \frac{\pi R^{\neq 2}}{\sigma} \left(\frac{8kT}{\pi\mu}\right)^{1/2} N_A e^{-\Delta E_0^\ddagger/kT} \end{aligned} \quad 32.1.17^\circ$$

Given a few additional assumptions, this result is in the same form as the hard-core collision rate constant, $k_2 = \sigma_{\text{HC}} \bar{c}_{\text{rel}} N_A$, Eq. 31.3.25. The first assumption is that we associate the hard-core collision cross section $\sigma_{\text{HC}} = \pi d^2$ with $\pi R^{\neq 2}$ in Eq. 32.1.17°. For heteronuclear collisions, the symmetry number is one, in agreement with Eq. 31.3.25. For homonuclear collisions the factor of $\sigma = 2$ applies, in agreement with the factor of two in Eq. 31.3.18 for Z_{AA} . Secondly, from kinetic molecular theory, the relative speed of the particles in the collision is $\bar{c}_{\text{rel}} = (8kT/\pi\mu)^{1/2}$. Finally, the exponential term relates the relative collisional kinetic energy to the energy barrier, ΔE_0^\ddagger . The extension of the hard-core collision relationship with this threshold activation term resolves a deficiency of the basic KMT approach. When applied to collisions of spherical structureless particles, ACT and hard-core collision theory are consistent, with the addition of threshold activation.

Multiple Crossings, Coupling of Degrees of Freedom, and Tunneling Are Neglected: Numerous comparisons of ACT have been made to experiment. The principle difficulty in applying ACT is in predicting the structure of the activated complex and in estimating the vibrational frequencies of the normal modes, Table 32.1.1. Historically, the ΔE_0^\ddagger zero-point energy shift was also difficult to calculate. As an expedient, ΔE_0^\ddagger was assumed to be equal to the experimentally determined activation energy. As a result, comparing the Arrhenius equation, $k_2 = A e^{-E_a/RT}$, to Eq. 32.1.14° gives the pre-exponential factor as:

$$A \cong \frac{kT}{h} \frac{q^{\neq 0}/N_A}{(q_A^0/N_A)(q_B^0/N_A)} \left(\frac{RT}{P^\circ} \right) \quad 32.1.18^\circ$$

Table 32.1.1: Experimental Tests of Activated Complex Theory, Eq. 32.1.14°. The presumed geometry of the activated complex is shown.¹⁻³

Reaction	E_a (kJ mol ⁻¹)	A (exp) (L mol ⁻¹ s ⁻¹)	A (theory)
NO + O ₃ → NO ₂ + O ₂ 	10.5	0.79 x 10 ¹²	0.4 x 10 ¹²
NO ₂ + CO → NO + CO ₂ 	132	12.6 x 10 ¹²	6.3 x 10 ¹²
2 ClO → Cl ₂ + O ₂ 	0.0	0.063 x 10 ¹²	0.01 x 10 ¹²

As seen in Table 32.1.1, experimental tests of activated complex theory typically show that theoretical predictions are too small by factors of two to six or more. By obtaining good order of magnitude estimates, ACT represents a significant accomplishment. However, the goal is to develop accurate theories of reaction dynamics. The underestimates have many potential causes. The basic assumption of ACT is that the activated complex crosses the transition barrier only once in a successful reaction. We will see that detailed reaction dynamics calculations show that in some cases the activated complex exists for several vibrational periods along the reaction coordinate. In such cases, the activated complex crosses over the transition state barrier multiple

times before giving products or returning to reactants. These cases are said to show **multiple crossings** through the transition state barrier.

The disadvantage of using statistical mechanics to determine the concentration of the activated complex is that all degrees of freedom are presumed to be at equilibrium. The short lifetime of the activated complex may not allow all degrees of freedom to come to equilibrium.⁴ Instead, the collision energy might be portioned favorably into a few internal degrees of freedom. The statistical development of the reaction rate assumes degrees of freedom do not interact. However, having energy in rotation or extra energy above the zero-point in bending vibrations or in the non-reactive stretches might have a strong effect on the fate of the activated complex.⁴ For example, rapid rotation might help “throw” the activated complex towards products, depending on the masses of the atoms. Having extra energy in the bending vibration might aid the bond breaking and making processes.

ACT also neglects quantum mechanical effects along the reaction coordinate.⁴ For example, tunneling may occur through the transition barrier. Tunneling processes are especially important in the transfer of light particles such as hydrogen atoms and electrons. H-atom transfer reactions often proceed more rapidly than predicted by ACT because the H-atom nuclei, which are just protons, tunnel through the reaction barrier. An additional difficulty inherent in ACT is that the relationship between the experimental activation energy and the quantum mechanical zero-point energy shift, ΔE_0^\ddagger , is not well-defined.

Extensive progress has been made towards improvements in ACT and other reaction dynamics approaches. However, before we consider some of those approaches we next discuss a thermodynamically inspired simplification of ACT that is particularly useful in organic chemistry and biochemistry.

Example 32.1.1: Activated Complex Theory

Determine the pre-exponential factor of the reaction $\text{O} + \text{H}_2 \rightarrow \text{OH} + \text{H}$ at 500 K. The transition state is linear, $(\text{O}\cdots\text{H}\cdots\text{H})^\ddagger$, with $R_{\text{OH}} = 1.137 \text{ \AA}$ and $R_{\text{HH}} = 0.983 \text{ \AA}$. The corresponding rotational constant is $\tilde{B}_e = 7.414 \text{ cm}^{-1}$. The doubly degenerate bend is at 709 cm^{-1} and the symmetric stretch is at 1484 cm^{-1} . The transition state is a $^3\Pi$ term,⁵ giving the degeneracy as $g^\ddagger = 6$. The electronic partition function of O-atoms at high temperature is estimated as $q_e(\text{O}) = 9$, Table 30.1.2. The experimental activation energy is 37.2 kJ mol^{-1} .⁶

Answer: The pre-exponential factor is given by Eq. 32.1.18°, which factors into translational, rotational, vibrational, and electronic partition function ratios. The translational partition function ratio is given using Eq. 30.2.19°:

$$\frac{q_t^{\ddagger\circ}/N_A}{(q_{t,A}^\circ/N_A)(q_{t,B}^\circ/N_A)} = \frac{N_A h^3}{V_m^\circ} \frac{1}{(2\pi kT)^{3/2}} \left(\frac{m^\ddagger}{m_A m_B}\right)^{3/2} = \frac{N_A}{(2\pi\mu kT/h^2)^{3/2} V_m^\circ} \quad 32.1.19^\circ$$

with $m^\ddagger = m_A + m_B$ and μ the collision reduced mass. With $\text{O} + \text{H}_2 \rightarrow (\text{O}\cdots\text{H}\cdots\text{H})^\ddagger$, μ is:

$$\mu = \left(\frac{m_A m_B}{m_A + m_B}\right)^{3/2} = \frac{(15.9994 \text{ g mol}^{-1})(2.01588 \text{ g mol}^{-1})}{15.9994 \text{ g mol}^{-1} + 2.01588 \text{ g mol}^{-1}} \left(\frac{1}{N_A}\right) (1 \text{ kg}/1000 \text{ g}) = 2.973 \times 10^{-27} \text{ kg}$$

The standard state volume is $RT/P^\circ = 0.083145 \text{ bar L K}^{-1} \text{ mol}^{-1} \cdot 500 \text{ K}/1 \text{ bar} = 41.57 \text{ L mol}^{-1} = 0.04157 \text{ m}^3 \text{ mol}^{-1}$. We used $R = 0.083145 \text{ L bar K}^{-1} \text{ mol}^{-1}$ because we want the concentrations in the rate law to be expressed in molar, mol L^{-1} , terms. The translational partition function ratio is:

$$\begin{aligned} \frac{N_A}{(2\pi\mu kT/h^2)^{3/2} V_m^\circ} &= \\ &= \frac{6.022 \times 10^{23} \text{ mol}^{-1}}{[2\pi \cdot 2.973 \times 10^{-27} \text{ kg} (1.3806 \times 10^{-23} \text{ J K}^{-1})(500.0 \text{ K})/(6.626 \times 10^{-34} \text{ J s})^2]^{3/2} \cdot 0.04157 \text{ m}^3 \text{ mol}^{-1}} \\ &= 2.878 \times 10^{-6} \quad (\text{translation}) \end{aligned}$$

Translation favors reactants. The spectroscopic constants for H_2 are in Table 27.6.1. The rotational constant for H_2 is 60.853 cm^{-1} with $\sigma_{\text{H}_2} = 2$. The transition state is unsymmetrical giving $\sigma^\ddagger = 1$. The rotational partition function ratio is:

$$\frac{q_r^\ddagger}{(q_{r,A})(q_{r,B})} = \frac{q_r^{\ddagger o'}}{q_{r,\text{H}_2}^o} = \frac{1/\sigma^\ddagger \tilde{B}^\ddagger}{1/\sigma_{\text{H}_2} \tilde{B}_{\text{H}_2}} = \frac{1/7.414 \text{ cm}^{-1}}{1/2(60.853 \text{ cm}^{-1})} = 16.416 \quad (\text{rotation})$$

Rotation favors the transition state, since the transition state has a large moment of inertia. The stretching vibration of H_2 and the symmetric stretch of the transition state are too energetic to contribute significantly to the pre-exponential factor, which leaves just the degenerate bend of the transition state. The factor of $kT/hc = 347.5 \text{ cm}^{-1}$ at 500 K:

$$\frac{q_v^\ddagger}{(q_{v,A})(q_{v,B})} \cong (q_{\text{bend}}^\ddagger)^2 = \left(\frac{1}{1 - e^{-hc\tilde{\nu}/kT}} \right)^2 = \left(\frac{1}{1 - e^{-709/347.5}} \right)^2 = 1.321 \quad (\text{vibration})$$

Vibration favors the transition state because of the extra low-frequency vibrational degrees of freedom. At high temperature, the electronic partition functions are assumed to be given by the electronic degeneracies of the ground state configurations: $g_{\text{O}} = 9$, $g_{\text{H}_2} = 1$, and $g^\ddagger = 6$:

$$\frac{q_e^\ddagger}{(q_{e,A})(q_{e,B})} \cong 6/9 = 2/3 \quad (\text{electronic})$$

At 500 K, $kT/h = 1.048 \times 10^{12} \text{ s}^{-1}$ so that the pre-exponential factor using Eq. 32.1.18° is:

$$\begin{aligned} A &\cong \frac{kT}{h} \frac{q^{\ddagger o'}/N_A}{(q_A^o/N_A)(q_B^o/N_A)} \left(\frac{RT}{P^\circ} \right) \\ &= 1.048 \times 10^{12} \text{ s}^{-1} (2.878 \times 10^{-6}) (16.416) (1.321) (2/3) (41.57 \text{ L mol}^{-1}) = 1.80 \times 10^{10} \text{ L mol}^{-1} \text{ s}^{-1} \\ &\quad \text{reaction coordinate} \quad \text{translation} \quad \text{rotation} \quad \text{vibration} \quad \text{electronic} \quad K_p \rightarrow K_c \end{aligned}$$

At 500 K, the rate constant is $k_2 = A e^{-E_a/RT} = 2.32 \times 10^6 \text{ L mol}^{-1} \text{ s}^{-1}$. This reaction has been extensively studied because of its importance in combustion and atmospheric processes.⁶⁻⁸ The $^3\Pi$ transition state corresponds to two degenerate states that separate upon bending and have significantly different PE surfaces, bending frequencies, and hence reaction rates.

Thermodynamic Transition State Theory Defines the Gibbs Energy of Activation: Activated complex theory as represented by Eq. 32.1.14° is useful in providing insight into the properties of the transition state. However, quantitative applications of ACT are difficult. A useful approach

that maintains the insights inherent in ACT while making the theory easy to apply to complicated reactions is **thermodynamic transition state theory**. The basic form of Eqs. 32.1.8° and 32.1.13° is maintained. We assume the activated complex is in equilibrium with the reactants with equilibrium constants K_c^\ddagger and K_p^\ddagger and use the high temperature approximation for the reactive asymmetric stretch, Eq. 32.1.13°:

$$k_2 = \frac{kT}{h} K_c^\ddagger = \frac{kT}{h} \left(\frac{RT}{P^\circ} \right) K_p^\ddagger \quad (\text{bimolecular ideal gas}) \quad 32.1.20^\circ$$

The equilibrium constant of the formation of the activated complex is related to the **Gibbs energy of activation**, $\Delta_r G^{\circ\ddagger}$, by:

$$\Delta_r G^{\circ\ddagger} = -RT \ln K_p^\ddagger \quad 32.1.21$$

We now picture the reaction profile plotted against the Gibbs energy with the transition state barrier characterized by the Gibbs energy of activation, Figure 32.1.3a.

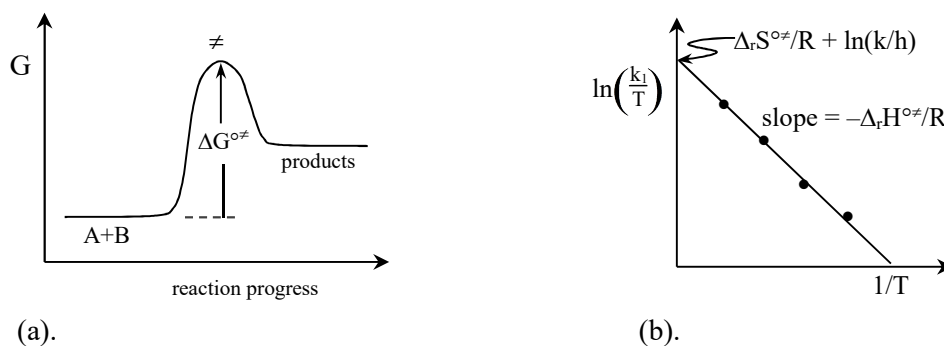


Figure 32.1.3: (a). The reaction profile is plotted versus Gibbs energy with the maximum giving the Gibbs energy of activation. (b). For unimolecular gas or solution reactions, the enthalpy and entropy of activation are determined from a plot of $\ln(k/T)$ vs. $1/T$.

Solving for the equilibrium constant in the last equation and substitution into Eq. 32.1.20° gives the bimolecular rate constant as:

$$k_2 = \frac{kT}{h} \left(\frac{RT}{P^\circ} \right) e^{-\Delta_r G^{\circ\ddagger}/RT} \quad (\text{bimolecular ideal gas}) \quad 32.1.22^\circ$$

In practice, this expression defines the Gibbs energy of activation. Another useful perspective is obtained by splitting the Gibbs energy into the corresponding enthalpy and entropy components. The **enthalpy and entropy of activation** are defined by:

$$\Delta_r G^{\circ\ddagger} \equiv \Delta_r H^{\circ\ddagger} - T\Delta_r S^{\circ\ddagger} \quad 32.1.23$$

Substitution of this last definition into Eq. 32.1.22° gives the **Eyring equation**, which separates the entropic and enthalpic effects upon the formation of the activated complex:

$$k_2 = \frac{kT}{h} \left(\frac{RT}{P^\circ} \right) e^{\Delta_r S^{\circ\ddagger}/R} e^{-\Delta_r H^{\circ\ddagger}/RT} \quad (\text{bimolecular ideal gas}) \quad 32.1.24^\circ$$

Even though Eqs. 32.1.22° and 32.1.24° are reminiscent of Arrhenius form, $k_2 = A e^{-E_a/RT}$, neither $\Delta_r G^{\circ\ddagger}$ nor $\Delta_r H^{\circ\ddagger}$ are equal to the activation energy. To find the relationship to the activation energy, we use the differential form of the Arrhenius expression, Eq. 4.5.25:

$$\left(\frac{\partial \ln k_2}{\partial T}\right)_V = \frac{E_a}{RT^2} \quad 32.1.25$$

To complete the derivative using Eq. 32.1.22°, we note that $RT/P^\circ = V^\circ$, which is the standard state volume. Finding the logarithm of Eq. 32.1.22° and taking the derivative gives:

$$\left(\frac{\partial \left(\ln \frac{kT}{h} + \ln V^\circ - \frac{\Delta_r G^{\circ\ddagger}}{RT}\right)}{\partial T}\right)_V = \frac{E_a}{RT^2} \quad 32.1.26^\circ$$

V° is constant since the derivative is taken at constant volume. The derivative of $\Delta_r G^{\circ\ddagger}/T$ with respect to T at constant volume is analogous to the derivative at constant pressure, which is the Gibbs-Helmholtz relationship, Eq. 16.3.12. The derivative at constant pressure is $-\Delta_r H^{\circ\ddagger}/T^2$, while the derivative at constant volume is $-\Delta_r U^{\circ\ddagger}/T^2$. $\Delta_r U^{\circ\ddagger}$ is the **internal energy of activation**. Eq. 32.1.26° then reduces to:

$$\frac{1}{T} + \frac{\Delta_r U^{\circ\ddagger}}{RT^2} = \frac{E_a}{RT^2} \quad 32.1.27^\circ$$

Solving for the activation energy gives: $E_a = \Delta_r U^{\circ\ddagger} + RT$. For ideal gas reactions we relate the internal energy and enthalpy using: $\Delta_r H^{\circ\ddagger} = \Delta_r U^{\circ\ddagger} + \Delta_r n_g RT$. For a bimolecular reaction the change in number of moles of gas upon forming the activated complex is $\Delta_r n_g = -1$. Solving for $\Delta_r U^{\circ\ddagger}$ and substituting this result into $E_a = \Delta_r U^{\circ\ddagger} + RT$ gives:

$$E_a = \Delta_r H^{\circ\ddagger} + 2RT \quad (\text{bimolecular ideal gas}) \quad 32.1.28^\circ$$

For a bimolecular reaction $\Delta_r H^{\circ\ddagger} = E_a - 2RT$, which with Eq. 32.1.24° gives the rate constant as:

$$k_2 = \frac{kT}{h} \left(\frac{RT}{P^\circ}\right) e^2 e^{\Delta_r S^{\circ\ddagger}/R} e^{-E_a/RT} \quad (\text{bimolecular ideal gas}) \quad 32.1.29^\circ$$

Comparing these relationships to the Arrhenius equation, $k_2 = A e^{-E_a/RT}$, gives the pre-exponential factor as:

$$A = \frac{kT}{h} \left(\frac{RT}{P^\circ}\right) e^2 e^{\Delta_r S^{\circ\ddagger}/R} \quad (\text{bimolecular ideal gas}) \quad 32.1.30^\circ$$

Thermodynamic transition state theory is commonly applied to reactions in solution. For either a unimolecular gas phase reaction or for reactions in solution $\Delta_r n_g = 0$ and $\Delta_r H^{\circ\ddagger} = E_a - RT$; using Eq. 32.1.7° gives:

$$k_1 = \frac{kT}{h} e^{\Delta_r S^{\circ\ddagger}/R} e^{-\Delta_r H^{\circ\ddagger}/RT} \quad (\text{unimolecular ideal gas or solution}) \quad 32.1.31^\circ$$

$$E_a = \Delta_r H^{\circ\ddagger} + RT \quad (\text{unimolecular ideal gas or solution}) \quad 32.1.32^\circ$$

$$k_1 = \frac{kT}{h} e^{e^{\Delta_r S^{\ddagger}/R}} e^{-E_a/RT} \quad (\text{unimolecular ideal gas or solution}) \quad 32.1.33^\circ$$

$$A = \frac{kT}{h} e^{e^{\Delta_r S^{\ddagger}/R}} \quad (\text{unimolecular ideal gas or solution}) \quad 32.1.34^\circ$$

In other words, the activation energy and enthalpy of activation differ by $\sim 2.5\text{-}5 \text{ kJ mol}^{-1}$ depending on the molecularity and state of aggregation. The linearized form of Eq. 32.1.31 $^\circ$ is obtained by dividing by T and taking the logarithm, Figure 32.1.3b:

$$\ln\left(\frac{k_1}{T}\right) = -\frac{\Delta_r H^{\ddagger}}{R} \left(\frac{1}{T}\right) + \frac{\Delta_r S^{\ddagger}}{R} + \ln\left(\frac{k}{h}\right) \quad (\text{unimolecular ideal gas or solution}) \quad 32.1.35^\circ$$

Typical bimolecular pre-exponential factors are in the range of $A = 10^{10} - 10^{11} \text{ L mol}^{-1} \text{ s}^{-1}$, which gives the entropy of activation using Eq. 32.1.30 $^\circ$ as $\Delta_r S^{\ddagger} \cong -80 \text{ J K}^{-1} \text{ mol}^{-1}$ (see Example 32.1.2). This strongly negative entropy of activation results because two reactants combine to form the one activated complex. This value is a good point of comparison with experiment in determining the molecularity of a mechanistic step. Reactions that have an entropy of activation more negative than -80 kJ mol^{-1} are presumed to have a strong orientation preference to give reactive collisions. Unimolecular processes have an activated complex that is more “loose and floppy” than the reactant. As a result, unimolecular processes are expected to be entropy neutral or have a positive entropy of activation, Table 32.1.2:

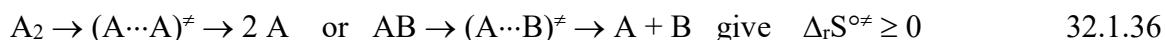
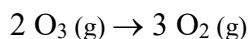


Table 32.1.2: Enthalpy and Entropy of Activation of Gaseous Reactions.⁹

Reaction	$\Delta_r H^{\ddagger}$ (kJ mol ⁻¹)	$\Delta_r S^{\ddagger}$ (kJ mol ⁻¹)
$O + O_3 \rightarrow 2 O_2$	17.53	-62.55
$N + O_2 \rightarrow NO + O$	21.37	-83.56
$2 CH_3 \rightarrow C_2H_6$	-5.82	-61.87
$N_2O_5 \rightarrow NO_3 + NO_2$	85.12	29.26
$CH_3CH_2Cl \rightarrow C_2H_4 + HCl$	230.83	-1.93
<i>cis</i> -CHCl=CHCl \rightarrow <i>trans</i> -CHCl=CHCl	227.45	-16.65

Example 32.1.2: Thermodynamic Transition State Theory

Find the activation enthalpy, entropy, and Gibbs energy of the decomposition of ozone at 298 K. The Arrhenius pre-exponential factor is $4.6 \times 10^{12} \text{ M}^{-1} \text{ s}^{-1}$. The activation energy is 10.0 kJ mol^{-1} :



Answer: Two handy constants at 298.15 K and 1 bar pressure are:

$$\frac{kT}{h} = 6.2124 \times 10^{12} \text{ s}^{-1} \quad \text{and} \quad \left(\frac{RT}{P^\circ}\right) = \frac{0.0831446 \text{ L bar K}^{-1} \text{ mol}^{-1} (298.15 \text{ K})}{1.000 \text{ bar}} = 24.7896 \text{ L mol}^{-1}$$

Using Eq. 32.1.30 $^\circ$ for the bimolecular pre-exponential factor with the given $A = 4.6 \times 10^{12} \text{ M}^{-1} \text{ s}^{-1}$ results in:

$$A = \frac{kT}{h} \left(\frac{RT}{P^\circ} \right) e^2 e^{\Delta_r S^\ddagger/R}$$

$$= 6.2124 \times 10^{12} \text{ s}^{-1} (24.7896 \text{ L mol}^{-1})(2.7183)^2 e^{\Delta_r S^\ddagger/R} = 4.6 \times 10^{12} \text{ L mol}^{-1} \text{ s}^{-1}$$

$$\text{or } e^{\Delta_r S^\ddagger/R} = 4.043 \times 10^{-3}$$

Solving for the activation entropy: $\Delta_r S^\ddagger = 8.3145 \text{ J K}^{-1} \text{ mol}^{-1} \ln(4.043 \times 10^{-3}) = -45.8 \text{ J K}^{-1} \text{ mol}^{-1}$

With Eq. 32.1.28^o: $\Delta_r H^\ddagger = E_a - 2RT$

$$\Delta_r H^\ddagger = 10.0 \text{ kJ mol}^{-1} - 2(8.3145 \text{ J K}^{-1} \text{ mol}^{-1})(298.15 \text{ K})(1 \text{ kJ}/1000 \text{ J})$$

$$= 10.0 \text{ kJ mol}^{-1} - 4.9579 \text{ kJ mol}^{-1} = 5.04 \text{ kJ mol}^{-1}$$

With Eq. 32.1.23: $\Delta_r G^\ddagger \equiv \Delta_r H^\ddagger - T\Delta_r S^\ddagger$

$$\Delta_r G^\ddagger = 5.04 \text{ kJ mol}^{-1} - (298.15 \text{ K})(-45.8 \text{ J K}^{-1} \text{ mol}^{-1})(1 \text{ kJ}/1000 \text{ J}) = 18.7 \text{ kJ mol}^{-1}$$

For pre-exponential factors in the range $A \sim 10^{10} - 10^{11}$ the entropy of activation is in the range:

$$e^{\Delta_r S^\ddagger/R} = 8.79 \times 10^{-6} \text{ to } 8.79 \times 10^{-5} \text{ giving } \Delta_r S^\ddagger = -96.8 \text{ to } -77.7 \text{ J K}^{-1} \text{ mol}^{-1}$$

or in round numbers $\sim -80 \text{ J K}^{-1} \text{ mol}^{-1}$.

The Transition State Geometry can be Determined Using Molecular Orbital Theory: ACT and similar theories generate the reaction profile within the Born-Oppenheimer approximation. Working within the Born-Oppenheimer approximation allows the properties of the transition state to be estimated using standard electronic structure codes. In electronic structure programs, the properties of the transition state are determined by a normal mode calculation. The transition state has the unique property that one and only one normal mode frequency is imaginary. The imaginary normal mode frequency results because the reactive normal mode coordinate has a maximum in energy and not a minimum. Some electronic structure programs list an imaginary frequency as a negative frequency, as a notational expedient. The transition state is located by adjusting the geometry until the normal mode calculation gives one and only one imaginary frequency. The ΔE^\ddagger of the reaction is the electronic energy of the transition state relative to the sum of the electronic energies of the reactants, after adding in the zero-point vibrational energies. Semi-empirical and low level *ab initio* approaches are only helpful while developing guesses for the geometry of the transition state. Meaningful results require advanced *ab initio* approaches with careful treatment of electron correlation. From the perspective of perturbation theory and configuration interaction, significant excited state character typically mixes into the transition state. Many transition states more closely resemble excited states of the reactants rather than the ground states of the reactants.

32.2 Potential Energy Surfaces for Reactive Collisions

Reaction dynamics theories such as ACT take a coarse-grained approach to molecular collisions. The properties of the transition state are taken as statistical averages over the rotational and vibrational degrees of freedom of the activated complex and over the motion along the reaction coordinate. A completely different approach is to model the reaction collision-by-collision, taking careful account of the motion along the reaction coordinate and the rotational and vibrational states of the activated complex. In **classical collision dynamics**, the collision is modeled as classical motion upon a quantum mechanical potential energy surface.

Consider an atom-diatom reaction such as Eq. 32.1.1:



To determine if a reaction occurs, we must follow the total energy as the reactants collide at the transition state. Before the reactants collide, each molecule has translational, rotational, and vibrational energy. During the collision, the energies of the reactants are combined into the translational, rotational, and vibrational energy of the transition state. If the energy in the transition state is partitioned, or funneled, into the reactive asymmetric stretch, bond breaking and making may occur. If the combined energy of the reactants is insufficient or if the energy flows into the wrong degrees of freedom, the transition state falls apart to produce reactants. The first step is to add some detail to the reaction profile plot, Figure 32.2.1. The reaction profile is the minimum energy path proceeding to products on the electronic potential energy surface. The total energy of the collision is the sum of the electronic, vibrational, rotational, and relative translational kinetic energy: $\epsilon_{\text{tot}} = \epsilon_{\text{elec}} + \epsilon_{\text{v}} + \epsilon_{\text{r}} + \epsilon_{\text{rel}}$. The relative translational kinetic energy is converted by the collision into energy in the reactive asymmetric stretch. The lowest possible vibrational energies are the zero-point vibrational energies: $\epsilon_{\text{v}} = \text{ZPE}$ for $\nu = 0$. For reaction Eq. 32.1.1, the zero-point energy of the reactants is for HF, the zero-point energy of the products is for H₂, and the zero-point energy of the activated complex is the sum of the degenerate bends and symmetric stretch. The translational energy is the difference $\epsilon_{\text{rel}} = \epsilon_{\text{tot}} - (\epsilon_{\text{elec}} + \epsilon_{\text{v}} + \epsilon_{\text{r}})$. The total energy is conserved during the collision. The total energy must exceed the transition state barrier, ΔE_0^\ddagger . The transition state barrier is related to the quantum mechanical barrier height, $\Delta \epsilon_{\text{b}}$, by the zero point energies of the reactants, $\text{ZPE}_{\text{react}}$, and the transition state, ZPR^\ddagger :

$$\Delta E_0^\ddagger = \Delta \epsilon_{\text{b}} + \text{ZPE}^\ddagger - \text{ZPE}_{\text{react}} \quad 32.2.1$$

The difference in energy at the zero-point vibrations for products and reactants is the reaction internal energy at absolute zero, $\Delta E_0 = \Delta_r U(0)$. The H + H-F reaction is endothermic.

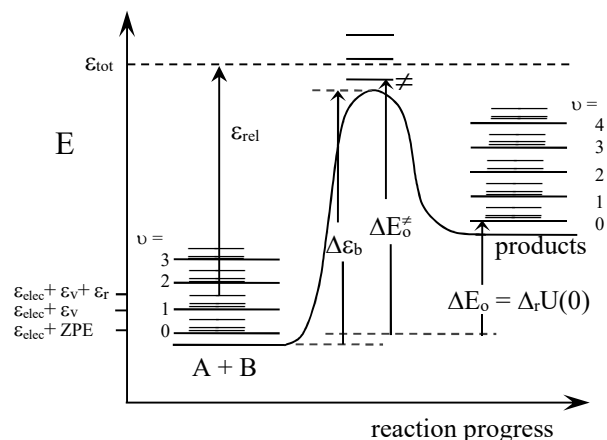


Figure 32.2.1: The reaction profile is plotted as the electronic energy only. The total energy (top dotted line) includes the relative translational kinetic energy, ϵ_{rel} . Total energy is conserved in the collision. The illustrated collision starts with the diatomic reactant in an excited rotational and vibrational state.

The Born-Oppenheimer Approximation is Assumed: The potential energy surface is generated within the Born-Oppenheimer approximation using electronic structure methods while varying the geometric parameters. Again, consider the H + HF reaction. We assume that the molecules don't rotate and that the molecules collide with the best orientation for a successful collision. Restricting the collision geometry greatly simplifies the calculations while retaining the important attributes of a reactive collision. The collision takes place along the bonding axis of the HF molecule and the H···H···F[‡] activated complex. This orientation is called a collinear collision. Other collision orientations have higher ΔE_0^\ddagger , making collinear the most important. The coordinate system for the reaction is given by the atom-atom distances, R_{HH} and R_{HF} :



The transition state occurs when R_{HH} is roughly equal to R_{HF} :



The potential energy surface is generated by determining the *ab initio* electronic energy as a function of R_{HH} and R_{HF} , Figure 32.2.2. The vertical axis in the perspective view is the electronic energy.

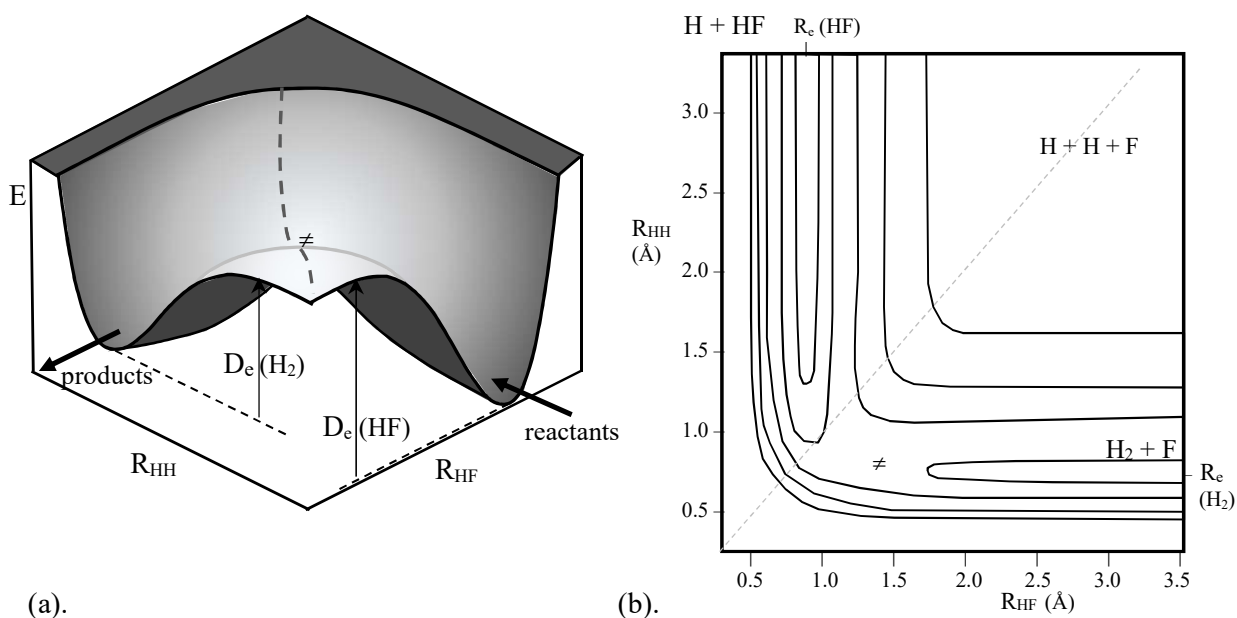


Figure 32.2.2: Potential energy surface for $\text{H} + \text{HF} \rightarrow \text{H}_2 + \text{F}$. (a). Perspective view. (b). Contour surface. The equilibrium bond lengths are at the bottom of the reactant ($\text{H} + \text{HF}$) and product potential energy valleys. Reactants start at the top of the diagram.

PE Surfaces Result in Stable Molecular Vibrations and the Reaction Coordinate: At large R_{HH} and large R_{HF} , the flat-plateau portion of the potential energy, PE, surface corresponds to

complete dissociation to atoms, $H + H + F$. The bond dissociation energy of HF is the depth of the reactant valley at large R_{HH} , as compared to the total dissociation limit, Figure 32.2.2a. The bond dissociation limit of H_2 is the depth of the product valley at large R_{HF} , as compared to the total dissociation limit. The bond dissociation energies of HF and H_2 are 6.126 eV and 4.749 eV, respectively. As a result, the $H + HF$ reaction is endothermic; the product valley is at higher energy than the reactant valley. As a consequence in the contour plot, more contour levels are required in the reactant valley as compared to the product valley, Figure 32.2.2b. At large R_{HH} , before the collision, the minimum of the PE valley is at the equilibrium bond length of HF. Motion at constant R_{HH} , which is the horizontal direction on the contour diagram, corresponds to the H–F stretch. At large R_{HF} , after a successful collision, the minimum of the PE valley is at the equilibrium bond length of H_2 . Motion at constant R_{HF} , which is the vertical direction on the contour diagram, corresponds to the H–H stretch. The reaction profile is the minimum energy path along the PE surface leading from reactants to products. The transition state is at the energy maximum along this path. The transition state is a **saddle-point**, Figure 32.2.3a. The surface is shaped like a saddle, which means that motion along the reaction coordinate is at a maximum, while motion perpendicular to the reaction coordinate is at a minimum. Motion perpendicular to the reaction coordinate corresponds to the symmetric stretch; both R_{HH} and R_{HF} increase and decrease together: $\overleftarrow{H}-H-\overrightarrow{F}$.

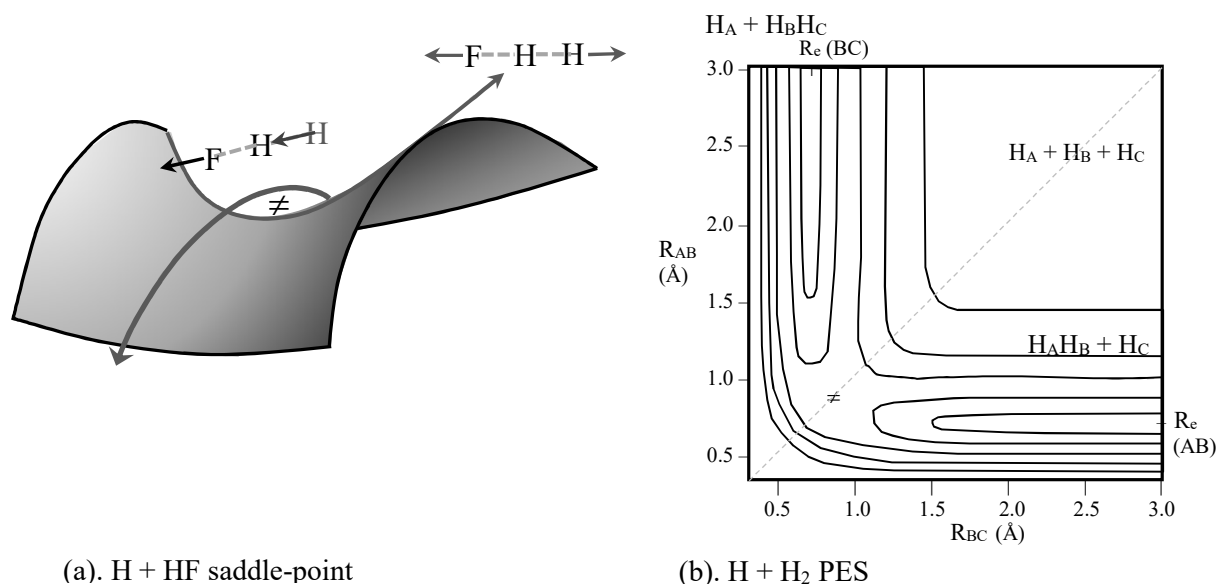
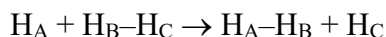


Figure 32.2.3: (a). The transition state is a saddle point along the reaction profile. The reaction coordinate is the reactive asymmetric stretch. Motion perpendicular to the reaction coordinate corresponds to the symmetric stretch, which has a minimum at the transition state. (b). The transition state for thermoneutral $H_A + H_B-H_C \rightarrow H_A-H_B + H_C$ is at $R_{AB} = R_{BC}$.

The Transition-State Saddle Point can be Early or Late: The gray dashed line in Figure 32.2.2b is at 45° , along which $R_{HH} = R_{HF}$. This line is positioned to highlight the relative location of the transition state. One reaction that has been extensively studied using classical collision dynamics is the very simple hydrogen-hydrogen atom-exchange reaction, Figure 32.2.3b:



32.2.4

Letter subscripts are given to differentiate the H-atoms, which are otherwise indistinguishable. Although seemingly trivial, this reaction displays many of the important attributes of all atom-diatom collisions. Because the products and reactants are the same, this reaction is necessarily thermo-neutral. The reactant and product valleys are of equal depth and the equilibrium bond lengths are identical. The PE surface of this reaction is symmetrical about the 45° line. As a result the transition state occurs on the 45° line. By comparison, the $\text{H} + \text{H}-\text{F}$ reaction has a **late transition barrier**. In other words, the transition state occurs on the product side of the 45° line. Late transition barriers often occur with endothermic reactions. Conversely the $\text{H} + \text{H}-\text{Br}$ reaction is exothermic and has an **early transition barrier**. The $\text{H} + \text{H}-\text{Br}$ transition state is on the reactants side of the 45° line. We will see that the position of the transition state has a significant effect on the energy demand and disposal of the reaction.

32.3 Classical Trajectory Calculations

Classical trajectory calculations simulate collisions by integrating Newton's equations of motion on the quantum mechanical potential energy surface. Consider a simple one-dimensional example of a harmonic oscillator. The potential energy of bond stretching is:

$$V = \frac{1}{2} \kappa (R - R_0)^2 \quad 32.3.1$$

where R is the current bond length, R_0 is the equilibrium bond length, and κ is the force constant of the bond. Simplifying Eq. 32.3.1, using the definition of the displacement $x \equiv R - R_0$, gives:

$$V = \frac{1}{2} \kappa x^2 \quad 32.3.2$$

The force that acts on the system is the negative of the derivative of the potential:

$$F = -\frac{dV}{dx} \quad 32.3.3$$

Taking the derivative of Eq. 32.3.2 gives:

$$F = -\kappa x \quad 32.3.4$$

which is Hooke's Law for a mass, m , on a spring with force constant κ . Newton's Law tells us that $F = ma$, where a is the acceleration. The acceleration is the rate of change of the velocity:

$$F = -\kappa x = m \frac{dv}{dt} \quad 32.3.5$$

The position of the system, x , is determined by integrating the equation:

$$\frac{dx}{dt} = v \quad 32.3.6$$

Integrating Eq. 32.3.5 gives the velocity as a function of time, with an initial velocity of v_1 :

$$\int_{v_1}^{v_2} dv = \int_{t_1}^{t_2} \frac{F}{m} dt \quad 32.3.7$$

Assuming the time interval is so short that the force is essentially constant over the time interval:

$$v_2 = v_1 + \frac{F}{m} (t_2 - t_1) \quad (\Delta t \text{ small}) \quad 32.3.8$$

For the specific case of a vibrating molecule m is replaced by the reduced mass, μ . Integrating Eq. 32.3.6 gives the position as a function of time, starting from an initial position of x_1 :

$$\int_{x_1}^{x_2} dx = \int_{t_1}^{t_2} v_2 dt \quad 32.3.9$$

Assuming the time interval is so short that the velocity is essentially constant over the time interval gives the position at time t_2 as:

$$x_2 = x_1 + v_2 (t_2 - t_1) \quad (\Delta t \text{ small}) \quad 32.3.10$$

Since the force, velocity, and position are all changing with time, Eqs 32.3.8 and 32.3.10 are solved repeatedly over short time steps, first updating the velocity and then updating the position. The value of x for each of these successive time intervals is the trajectory of the system. In molecular dynamics simulations the time step must be very short, usually $dt = t_2 - t_1 = 1 \times 10^{-15}$ s or 1 femtosecond, 1fs. Assuming that the force and velocity are constant over short time intervals during each time step is called the **finite difference approximation** to the solution of the differential equations. In classical trajectory calculations of H + HF as an example, Newton's equations are integrated over the two-dimensional potential energy surface. The coordinates are R_{HH} and R_{HF} . Eqs 32.3.8 and 32.3.10 must be modified for the two-dimensional problem, but otherwise the approach is the same; v and x become vectors.

Three collisions are illustrated in Figure 32.3.1. The collisions begin at the top of the PE surface diagrams. Classical trajectory calculations are often likened to rolling a marble or riding a skate board on the PE surface. The first collision has the HF molecule in the zero-point, $v = 0$, vibrational level and relative translational kinetic energy of 1.4 eV. The first collision is unsuccessful, returning to reactants, because the relative translational plus vibrational energy is less than the energy barrier.

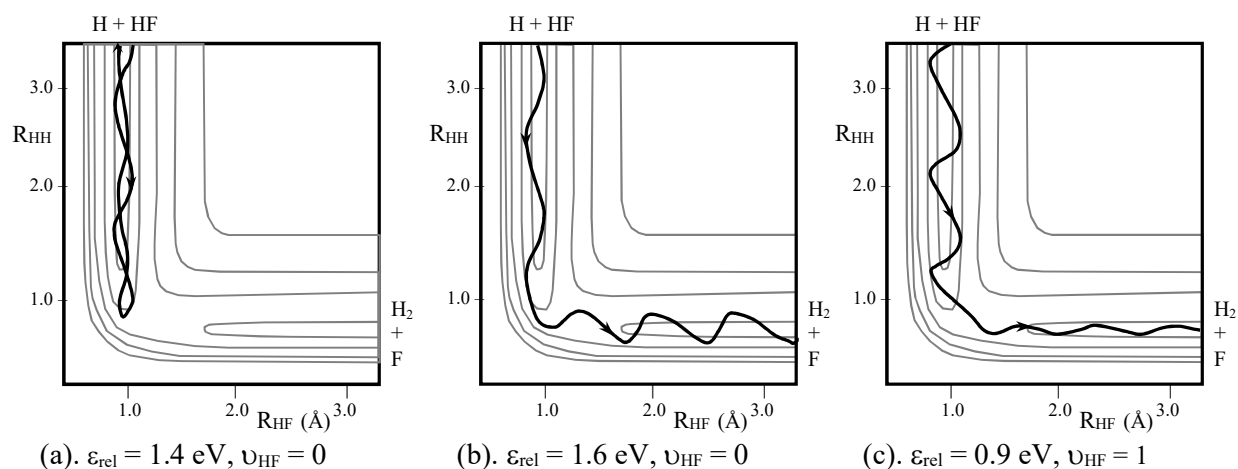


Figure 32.3.1: Classical trajectory calculations. (a). Unsuccessful collision, HF in $v = 0$: insufficient relative translational kinetic energy. (b). Successful collision, HF in $v = 0$: the product H_2 produced in an excited vibrational state. (c). Successful collision, HF in $v = 1$: the product produced in the zero-point vibrational state.

The second collision also has the HF molecule in the zero-point vibration level, but with relative translational energy increased to 1.6 eV. The second collision is successful. The third collision has the HF molecule in the $\nu = 1$ vibrational level, but the relative translational energy is reduced to 0.9 eV. This collision has insufficient translational energy, alone, to exceed the energy barrier. The third collision is successful, showing that the energy demand is satisfied by the sum of the relative translational and vibrational energy. The relative translational energy need not exceed the barrier on its own.

Figure 32.3.2 is another view of the successful trajectory in Figure 32.3.1b. The trajectory is plotted as a function of time. At the beginning, the R_{HH} distance is large. The initial values of R_{HF} oscillate about the HF equilibrium bond length in the reactant valley. A successful collision produces H_2 and the final values of R_{HH} oscillate about the H_2 equilibrium bond length in the product valley. A rough value of the time span of the transition region can be determined from the end of the time period with regular oscillations of the HF bond length to the onset of regular oscillations of the H_2 bond length. This region is underlined in the figure and lasts roughly 10-20 fs, that is only $\sim 20 \times 10^{-15}$ s. A collision with this type of smooth, direct traversal of the transition region is called a **direct** transition. Direct transitions are typical. The critical bond making and breaking events in many chemical reactions require an amazingly short period of time. The reason that reactions appear to be slow is that few collisions result in the formation of products, because of insufficient collision energy, improper orientation, or poor collision timing. The astoundingly short time period required for chemical change is a key insight that is shown by trajectory studies and molecular beam experiments (see below).

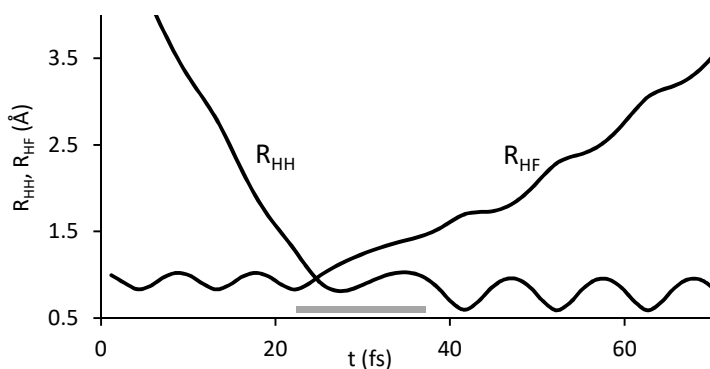


Figure 32.3.2: Trajectory in Figure 32.3.1b plotted as a function of time in femtoseconds. The transition region, underlined in gray, lasts roughly 10-20 fs.

The vibrational states of the reactant and product are determined by observing the amplitude of the vibration perpendicular to the reaction path. In the first and second trajectories in Figure 32.3.1, the amplitude of the initial vibration is small showing the initial zero-point vibrational states. In the third trajectory, the initial amplitude is significantly larger showing the $\nu = 1$ state. In the second trajectory, the final vibrational amplitude, in the vertical direction of the diagram, is large. The second trajectory produces product in an excited vibrational state. The product of the third collision is in the zero-point vibrational level. The partitioning of the energy of the products into translational kinetic energy or vibrational energy is called the **energy disposal**. Total energy of the collision is conserved, so that translational and vibrational energy compete for the overall energy disposal. The translational energy is determined using the spacing between

the vibrational maxima. Closely spaced vibrational maxima mean that the molecule hasn't moved very far during a vibrational period.

The third trajectory shows that the energy of a successful collision can be supplied by vibrational or translational energy. The partitioning of the initial energy as translational or vibrational energy is called the **energy demand**. Can we predict the energy demand and disposal of reactions?

Reaction Energy Demand and Disposal Depends on the Shape of the PE Surface: The second and third trajectories, Figure 32.3.1b-c, show that PE surfaces with a late barrier have a significantly lessened demand for translational energy when the reactant is in an excited vibrational state. For an additional comparison, consider a late barrier with two trajectories having equal total translational and vibrational energy, Figure 32.3.3a-b. Collisions at this total energy with zero-point vibrational energy are not successful, while collisions with $\nu = 1$ are successful.

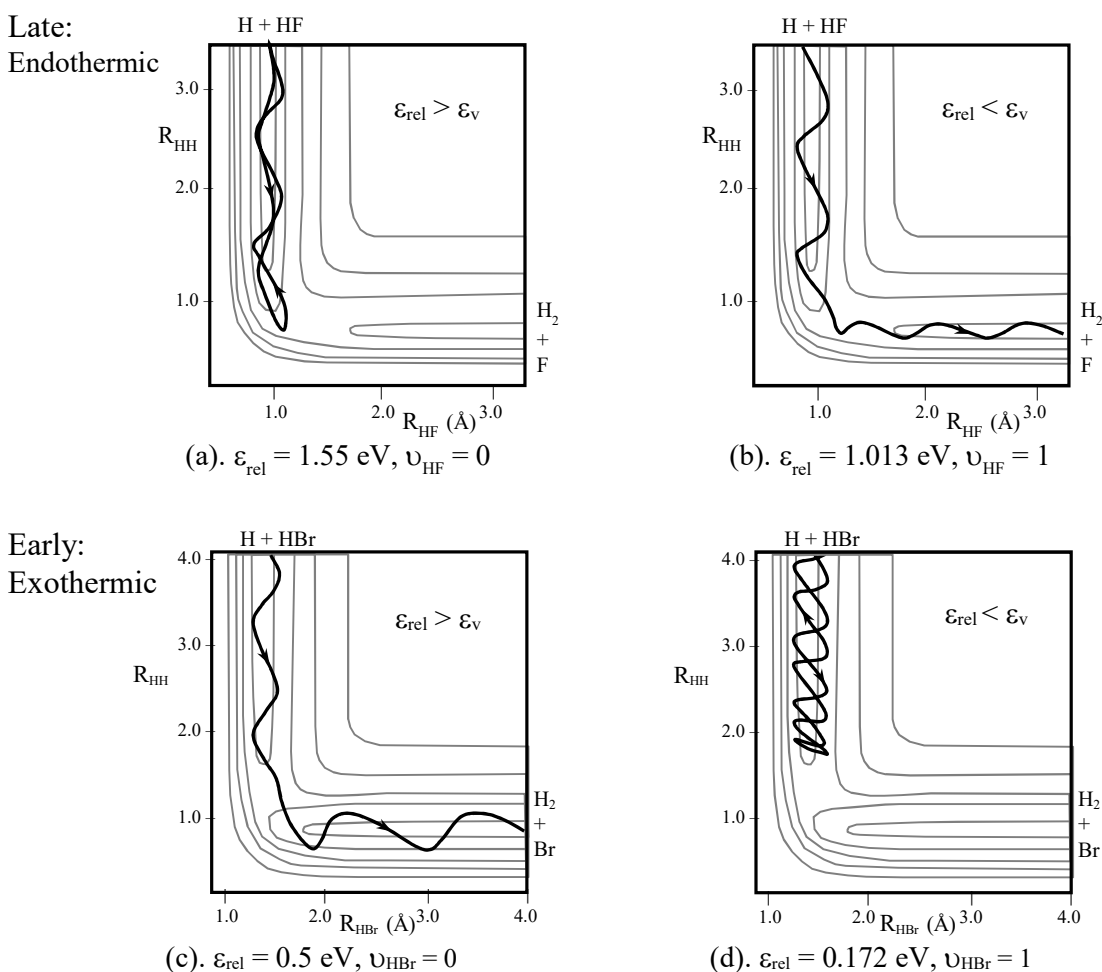


Figure 32.3.3: Trajectory pairs with equal total energy. Late barriers have an energy demand that favors vibration, while early barriers have an energy demand that favors translation.

(a). $\epsilon_{\text{rel}} + \epsilon_{\text{v}} = 1.55 + 0.268 \text{ eV} = 1.818 \text{ eV}$, (b). $\epsilon_{\text{rel}} + \epsilon_{\text{v}} = 1.013 + 0.805 \text{ eV} = 1.818 \text{ eV}$,
(c). $\epsilon_{\text{rel}} + \epsilon_{\text{v}} = 0.50 + 0.164 \text{ eV} = 0.664 \text{ eV}$, (d). $\epsilon_{\text{rel}} + \epsilon_{\text{v}} = 0.172 + 0.492 \text{ eV} = 0.664 \text{ eV}$

Consider an early barrier with two trajectories having equal total translational and vibrational energy, Figure 32.3.3c-d. Collisions at this total energy with zero-point vibrational energy are successful, while collisions with $\nu = 1$ are not successful. Late barriers have an energy demand that favors vibration, while early barriers have an energy demand that favors translation. In effect for late barriers, energy in vibration helps the trajectory turn the corner towards the transition state. For early barriers the transition state barrier is straight ahead along the reactant valley, favoring translational energy.

The energy disposal of the reaction is also predicted using the shape of the potential energy surface. Endothermic reactions have less energy available for vibration and rotation of the products than exothermic reactions. On this basis alone, the prediction is that exothermic reactions are more likely than endothermic reactions to produce products in excited vibrational states. In finer detail, endothermic reactions often have later barriers. Motion across the transition state is aligned along the product valley, Figure 32.3.3b. Little impetus exists for throwing the products in the perpendicular direction, which corresponds to vibration. Exothermic reactions often have early barriers. Motion across the transition state is perpendicular to the product valley, Figure 32.3.3c. Motion across the transition state often throws the products against the repulsive wall of the product valley, which corresponds to the large amplitude motion perpendicular to the product valley giving vibrational excitation. Summarizing, vibrational energy disposal is favored by early-barrier exothermic reactions and translational energy disposal is favored by late-barrier endothermic reactions.

The Timing of the Reaction During the Vibrational Period of the Reactant Matters: One of the most useful and surprising results of classical trajectory studies is that reaction timing can have a significant effect on the probability of reaction. Otherwise equivalent trajectories with the collision occurring at different phases of the HF vibration have different results, Figure 32.3.4.

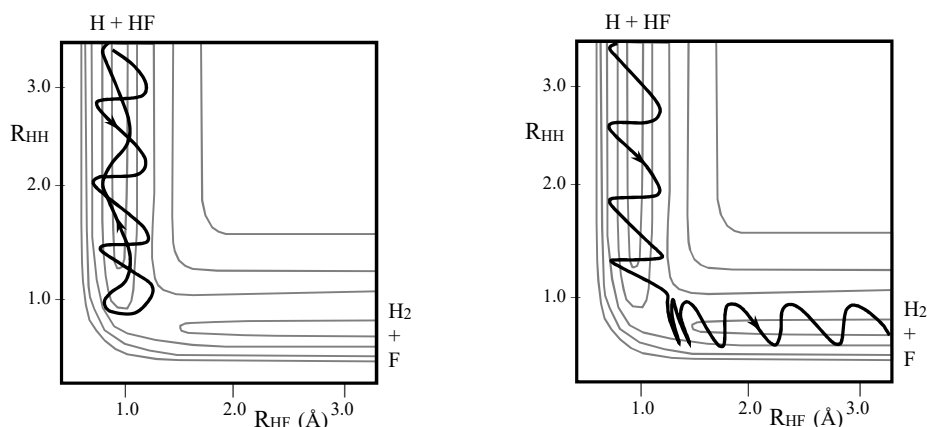


Figure 32.3.4: The timing of the collision with respect to the course of the vibrational motion is important for some collision conditions. The two trajectories have the same translational and vibrational energy and differ only in the initial R_{HH} distance. The collision occurs at different points, or phases, during the vibration.

For example, if the H atom approaches while the HF molecule is at its minimum internuclear distance, the reaction is less likely to occur, Figure 32.3.5. If the H atom approaches while the HF molecule is near its maximum internuclear distance, the leaving atom is already moving in

the right direction for bond breaking and the reaction is more likely to occur. In trajectory calculations the reaction probability is averaged over a uniform distribution of collision phases.

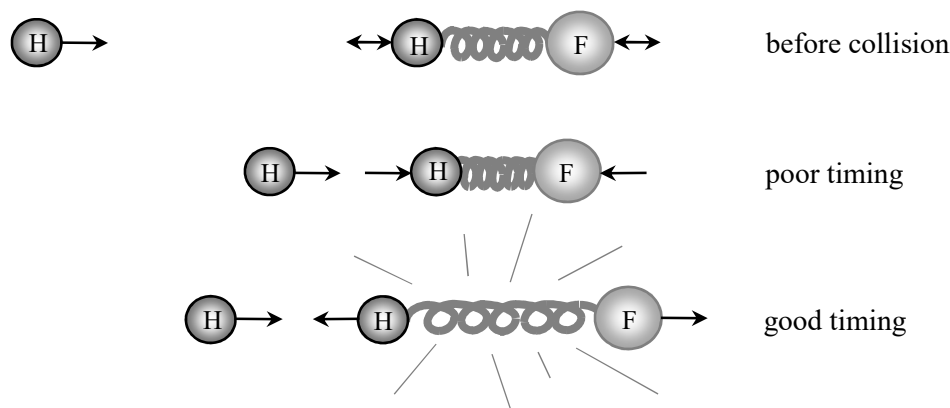


Figure 32.3.5. The effect of reaction timing on reactive collisions. Not all reactions with sufficient total energy are successful.

Some Conditions Give Multiple Crossings: The second trajectory in Figure 32.3.4 also shows that some trajectories cross the transition state dividing surface more than once. Many theories of reaction rates assume that once the activated complex crosses the transition state barrier that products always form. If the activated complex crosses the transition state barrier more than once, then we say that there are **multiple crossings**. Multiple crossings sometimes lead the activated complex to return to reactants; therefore such theories overestimate the rate of the reaction. However, even with multiple crossings the total time is a few vibrational periods.

Reactions in Solution and Enzyme Catalyzed Reactions are Treated Using Hybrid Molecular Dynamics: Classical trajectory calculations on quantum mechanical potential energy surfaces are one aspect of the much larger field of **molecular dynamics** simulation. Trajectories are often calculated on purely classical potential energy functions based on molecular mechanics force fields, Sec. 8.8. Molecular dynamics, MD, is a powerful approach to understanding processes in solution, in proteins and oligonucleotides, and at interfaces. MD simulation of reactions in solution or in enzyme catalysis requires a potential energy surface with thousands of dimensions. The use of purely quantum mechanical potential energy functions in MD simulations of solutions or enzymes is clearly impractical. However, hybrid methods are used for large systems, where parts of the system, such as the solvent, are treated using molecular mechanics force fields and the important coordinates along the reaction path are treated quantum mechanically.^{10,11} The examples we have discussed such as $\text{H} + \text{HF}$ are done on a potential energy surface that is prepared in advance of the MD simulation; the quantum mechanical results are fit to a parameterized surface based on the Morse potential (LEPS surfaces). For large systems this approach is impractical; rather the potential energy surface is generated “on the fly” by tightly integrating the quantum electronic structure and molecular dynamics algorithms. The electronic potential energies aren’t calculated until needed, at the current coordinates in the MD simulation.^{10,11} These hybrid or QC/MM molecular dynamics simulations have become the principle tool for extending the theories of gas phase reaction dynamics into systems of biochemical interest. So far we have been focusing on theoretical aspects of reaction dynamics. How do we ensure that our theoretical methods are on the right track?

32.4 Molecular Beams

Reactions can be Studied Collision by Collision: **Molecular beam scattering** experiments provide a collision by collision view of chemical reactions. These techniques are the experimental counterpart to classical trajectory studies. An amazing variety of molecular beam experiments are available. One of the first molecular beam experiments is typical. The reaction $\text{K} + \text{HBr} \rightarrow \text{KBr} + \text{H}$ is studied by forming a narrow beam of K-atoms which collide with a narrow beam of HBr molecules with a collision angle of 90° , Figure 32.4.1. Such a collision geometry is called a **crossed molecular beam** experiment. Molecular beams are formed by expansions of a gas through a small hole or nozzle with the beam divergence being narrowed by one or several skimmers that are placed in the beam, Figure 32.4.1b. Beams of alkali metal atoms are easily formed by placing the metal in a small oven with a hole. The velocity of either of the reactants can be selected using a velocity selector, which are spinning disks with offset slots, Figure 32.4.1c. At a given rotation speed, only molecules with the proper velocity can pass through the slots in both disks. Higher velocities are selected by higher rotation speeds. The orientation and rotational states of molecular reactants can also be selected using inhomogeneous electric fields. Excited vibrational states can be produced by laser irradiation. The products of the reaction are determined as a function of scattering angle by a movable detector that is mounted on an arc surrounding the collision region. Use of a mass spectrometer as a detector allows the identity of the products to be determined. The velocity of the products is also often determined. The vibrational state of the products is determined using infrared emission or by laser induced fluorescence. The entire apparatus must be held at high vacuum to ensure the mean free path of all species is greater than the instrument dimensions.

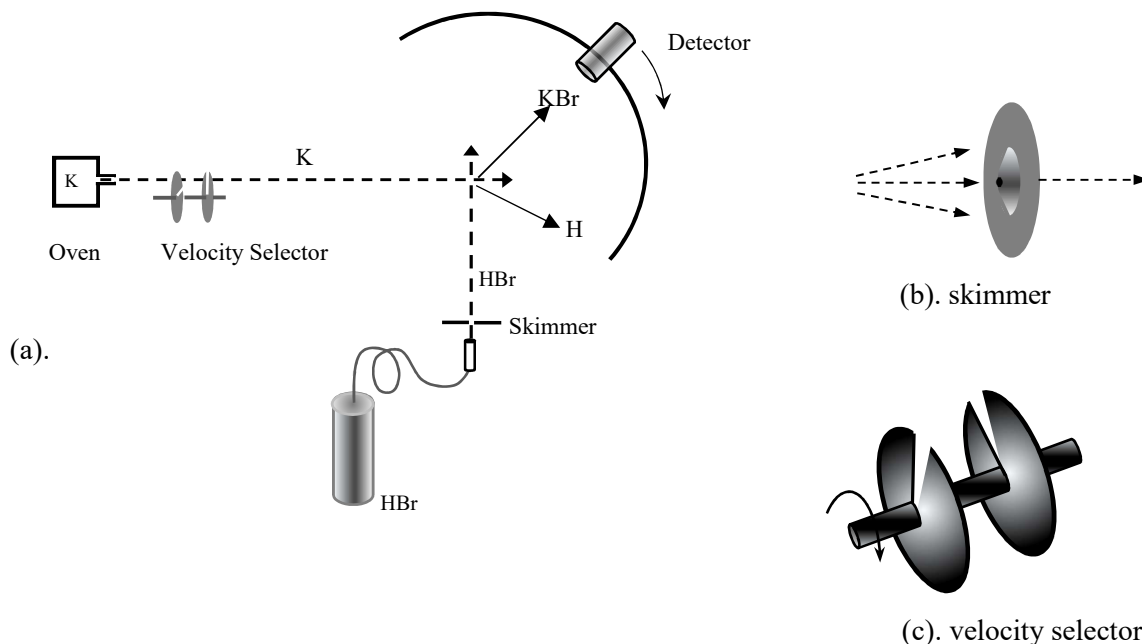


Figure 32.4.1: Crossed molecular-beam scattering. (a). A heated oven is the source of K atoms and a nozzle is the source of HBr molecules which meet with a 90° collision geometry. (b). Skimmers are metal disks with conical cross section and a small hole, which may be used in either beam to narrow the beam divergence. (c). Velocity selectors are spinning disks with offset slots, which may be used in either beam to select a narrow range of velocities.

The Scattering Angular Distribution Depends on the Potential Energy Surface: The angular dependence of the products of a molecular beam experiment is determined in the “laboratory” frame of reference. Collisions are best discussed in the center of mass frame of reference, Sec. 32.5. In the center of mass frame of reference, the collision partners approach with trajectories opposed at 180° , $\rightarrow \leftarrow$, Figure 32.5.1. The conversion of the laboratory-frame angular distribution to the center of mass frame of reference is geometrically detailed. For our purposes, we just present some of the results of molecular beam experiments. Most importantly, the intermolecular potential energy function can be determined from a detailed analysis of the velocity profile of the scattering angular distribution.

The scattering distribution is in part determined by the lifetime of the transition state. Long lived transition states give little preference for scattering direction. The long lifetime of the transition state allows the activated complex to undergo many rotations before falling apart. An example is the reaction $\text{H} + \text{CN} \rightarrow \text{HC} + \text{N}$. The HCN transition state corresponds to a stable molecule. While an inherently stable species, the HCN formed in the collision must dissociate because of conservation of energy. The transition state has too much total energy to remain bound. However, the stability of HCN gives a minimum on the potential energy surface and a long-lived transition state.

Transition states with short lifetimes tend to give scattering with narrow angular distribution, which are characterized as being in the “forward” or “backwards” directions, in the center of mass reference frame. Stripping type-mechanisms typically give forward scattering and rebound type-mechanisms give backward scattering, Figure 32.4.2. Several examples help to clarify the relationships.

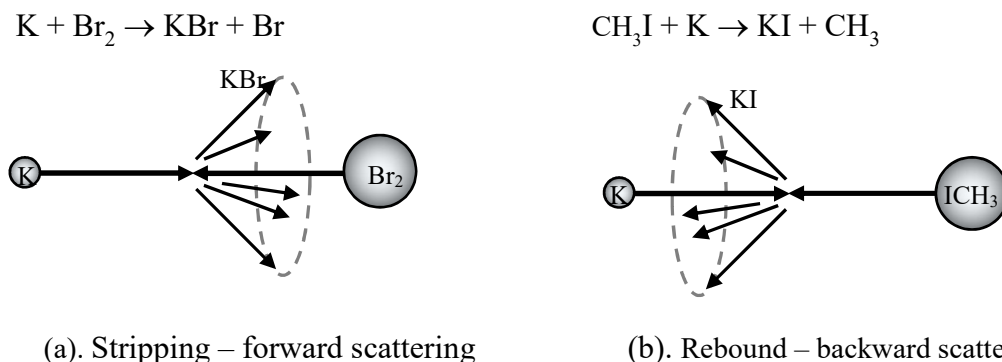
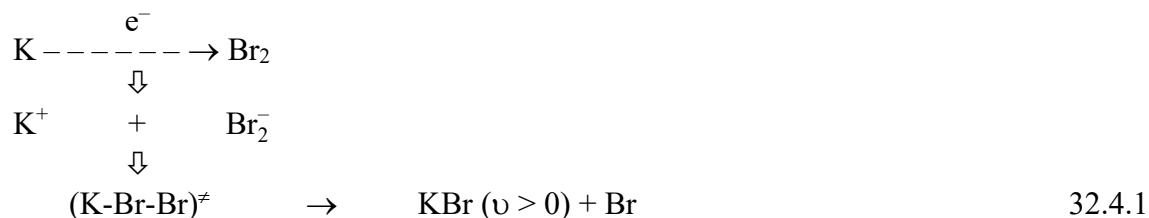


Figure 32.4.2: (a). A stripping type-collision gives scattering in the “forward” direction with respect to the incident K-atom. (b). A rebound type-collision gives scattering in the “backward” direction with respect to the incident K-atom. The K-atom is much less massive than the CH_3I molecule.¹²

The $\text{K} + \text{Br}_2 \rightarrow \text{KBr} + \text{Br}$ is an example of a stripping collision. The experimental reaction cross-section is factor of 4.8 larger than the hard-core collision cross-section. The large reaction cross-section results because an electron is transferred between the reactants at long distances. After the charge transfer, the K^+ and Br_2^- ions experience a strong Coulomb attraction that accelerates the ions towards each other:



In effect, the electron is stripped from the K-atom by the Br₂ molecule. Because the electron is very light compared to the collision partners and the resulting Coulomb attraction is strong, the momentum of the collision is carried forward, Figure 32.4.2a. This particular stripping mechanism is called the **harpoon** mechanism, because after the electron is “shot” between the collision partners, the resulting strong attraction pulls the partners together, giving a reaction cross-section bigger than the hard-core cross section. The reaction is strongly exothermic. After the collision, the product KBr is produced in a vibrationally excited state, as is often the case with exothermic reactions.

H-atom transfer reactions are also examples of stripping collisions. In the Cl + HI → I + HCl reaction, an H-atom is transferred between two heavy atoms in a short-lived transition state. Because the H-atom is much lighter than the I-atom, the I-atom momentum remains essentially unchanged during the collision, which carries the momentum in the forward direction. The heavy atoms are **spectators** during the light atom transfer. As spectators, the momenta are little changed by the transfer of the H-atom. The reaction is strongly exothermic, and correspondingly gives products in excited vibrational states. The HCl vibrational state with the maximum probability is $\nu = 3$.

The K + CH₃I → KI + CH₃ reaction has a rebound type-mechanism, Figure 32.4.2b. The heavy K-atom collides with the heavier CH₃I molecule. The momenta of the heavy particles is reversed, similar to collisions of billiard balls, which gives backwards scattering.

Velocity selection of the reactants allows the reaction cross-section to be determined as a function of collision kinetic energy. As we will discuss in Sec. 32.7 reaction cross-sections are strongly energy dependent. For many reactions, the cross-section is small near the relative energy threshold, proceeds through a maximum, and returns to small values at very high collision energies.

One difficulty in comparing molecular beam measurements with theoretical trajectory calculations is that molecules are rapidly rotating in a wide range of rotational levels near room temperature. However, using molecular beams formed using rapid expansion through small nozzles provides a unique opportunity. The expansion of a gas starting at pressures on the order of 100 torr through a small nozzle into a vacuum provides an adiabatic expansion that cools the molecules in the beam to low temperature. The molecules travel along the beam direction near supersonic velocities, giving a **supersonic expansion**. At the low temperatures produced, most molecules are in low lying rotational J-states within the zero-point vibrational level. Even though traveling at high velocity along the direction of the beam, supersonic expansion creates a low translational temperature transverse to the beam. This low transverse temperature greatly decreases the collision rate within the beam, which slows collisional rotational and vibrational energy transfer. As a result, microwave absorption can be used to excite molecules into specific rotational states for use in scattering experiments. Supersonic expansion also allows the formation of molecular complexes that are disrupted by collisions at room temperature. Complexes that are bound only by Van der Waals forces can easily be studied in supersonic

expansions, which yields useful experimental information on these important intermolecular forces.

Molecular beam experiments are necessary for validating reaction dynamics theories. High levels of electronic structure theory are needed to reproduce the results of molecular beam experiments. Theory development in reaction dynamics is progressing at a rapid pace as a result of the detailed information available from molecular beam studies.

*Break-down of the Born-Oppenheimer Approximation:*¹² All chemical reactions that require bond scission result from the break-down of the Born-Oppenheimer approximation, as discussed in Secs. 28.2 and 28.9. The vibrations of the molecular reactants and products in a reaction occur on different adiabatic, Born-Oppenheimer surfaces. The systems jumps or crosses-over from the reactant to the product potential energy surface at the transition state. The harpoon mechanism of the reaction, $\text{K} + \text{Br}_2 \rightarrow \text{KBr} + \text{Br}$, is an example of a non-adiabatic curve-crossing. The potential energy curves of the $\text{K} + \text{Br}_2$ reactants and $\text{K}^+ \cdots \text{Br}_2^-$ ion-pair cross at large distances, Figure 32.4.3. The $\text{K} + \text{Br}_2$ potential is relatively constant at large $\text{K} - \text{Br}_2$ distances. The $\text{K}^+ + \text{Br}_2^-$ potential energy surface is dominated by the Coulomb potential at large distances. The avoided-crossing, which carries the reaction from the $\text{K} + \text{Br}_2$ surface to the ion-pair, results from long-distance electron transfer. The electronic energy is coupled to the nuclear motion.

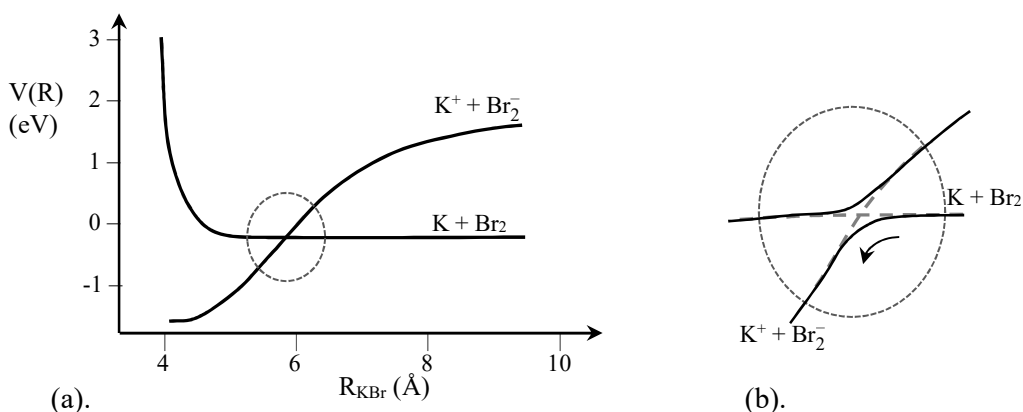


Figure 32.4.3: (a). Curve-crossing between the $\text{K} + \text{Br}_2$ and $\text{K}^+ \cdots \text{Br}_2^-$ potential energy surfaces. (b). Avoided-crossing carries the collision from the $\text{K} + \text{Br}_2$ to the $\text{K}^+ \cdots \text{Br}_2^-$ surface, which corresponds to the long distance electron transfer. (Adapted from Ref. 12)

We have been working hard to characterize bimolecular reaction dynamics, all the while ignoring unimolecular processes. Our theories of the transition state in bimolecular dynamics inform our understanding of equally important unimolecular processes.

32.5 Unimolecular Processes

Unimolecular processes have long been intriguing.¹³ At first glance mono-molecularity suggests that only one molecule is involved, just the reactant. However, the Lindemann-Henshelwood mechanism, Example 4.2.2, shows that as long as the unimolecular decomposition is the rate limiting step, the process can still be activated by molecular collisions:



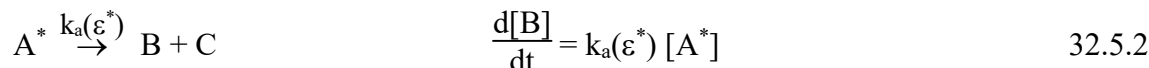
However, the unimolecular step must be the slow step. But if the activated molecule, A^* , has sufficient energy to react, why does it not promptly fall apart? Why is unimolecular decomposition often slow? Unimolecular processes also occur after photochemical excitation to an excited state:



After excitation, the primary photochemical dissociation or isomerization can be a slow process. Pre-dissociation, which is one possible unimolecular pathway, often requires multiple vibrational periods before avoided curve-crossing generates products. While sufficient energy exists after the initial collision or photochemical excitation, some time must be required for the available energy to funnel into the reactive asymmetric stretch that constitutes the reaction coordinate. During this time interval, the activated reactant is susceptible to vibrational relaxation caused by collisions and internal conversion, which generate the ground state reactant and heat, Sec. 28.6. One advantage of studying photochemical unimolecular processes is that the excitation energy can be easily controlled, simply by changing the wavelength of the incident light.

Unimolecular photochemical processes have common characteristics with fluorescence. In fluorescence, internal conversion involves energy transfer to high energy vibrational states of the ground state. At high energies, vibrational levels form a continuum of states. Can a unimolecular process be modeled similarly, with consideration of the high energy vibrational continuum of the activated molecule? Internal conversion and unimolecular reactions are necessarily non-adiabatic, because the unimolecular transition state must cross from the reactant to the product potential energy surfaces.

The energy levels involved are shown in Figure 32.5.1. The probability of unimolecular reaction depends on the excitation energy. Consider an activated molecule with excitation energy ϵ^* . The excitation energy must be greater than the zero-point energy shift ΔE_0^+ that forms the barrier. We wish to calculate the unimolecular rate constant $k_a(\epsilon^*)$ for a range of excitation energies from ϵ^* to $\epsilon^* + d\epsilon$. For chemical reactions, the unimolecular rate constant, k_1 , is the thermal average of $k_a(\epsilon^*)$ over the excitation energy distribution. The rate law of production of products for the given excitation energy range is then:



The activated molecule progresses to the transition state. For unimolecular processes the analog of the activated complex is called the **critical configuration**, A^\ddagger . The critical configuration can progress along the reaction coordinate to form products or fall back to A^* at a rate given by the frequency of the reactive asymmetric stretch, ν^\ddagger . Following our derivation of transition state theory, the activated molecule and the critical configuration may be considered to be in equilibrium:



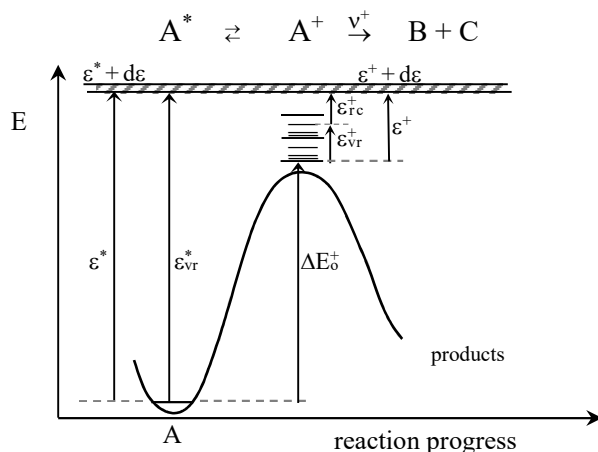


Figure 32.5.1: Energy relationships in a unimolecular reaction.¹³ The excitation energy ε^* must be greater than ΔE_0^+ to form an activated molecule, A^* . The excitation energy in the activated molecule is in vibration and rotation, ε_{vr}^* . The energy in the critical configuration, A^+ , is in vibration, rotation, and the reaction coordinate: $\varepsilon^+ = \varepsilon^* - \Delta E_0^+ = \varepsilon_{vr}^+ + \varepsilon_{rc}^+$.

The equilibrium constant for the formation of the activated complex is $K^+ = [A^+]/[A^*]$. This equilibrium constant is given by the ratio of the number of accessible states of the critical configuration divided by the number of accessible states of the activated reactant. The energy available to the critical configuration is $\varepsilon^+ = \varepsilon^* - \Delta E_0^+$. Over the narrow excitation energy range $d\varepsilon$, the number of assessable states is given by the density of states. The density of states of the activated molecule is at energy ε^* and the density of states of the critical configuration is at energy ε^+ , Figure 32.5.1:

$$K^+ = \frac{[A^+]}{[A^*]} = \frac{\rho^+(\varepsilon^+)}{\rho^*(\varepsilon^*)} \quad 32.5.4$$

The rate law for the unimolecular formation of products in terms of v^+ is then:

$$\frac{d[B]}{dt} = v^+ [A^+] = v^+ K^+ [A^*] \quad 32.5.5$$

Comparing Eqs. 32.5.2, 32.5.4, and 32.5.5 gives the unimolecular rate constant with excitation energy ε^* :

$$k_a(\varepsilon^*) = v^+ \frac{\rho^+(\varepsilon^+)}{\rho^*(\varepsilon^*)} \quad 32.5.6$$

The density of states of the critical configuration is given by the product of the density of states of the reactive asymmetric stretch, $\rho_{rc}(\varepsilon^+)$, and the density of states of the remaining rotational and vibrational degrees of freedom, $\rho^{+i}(\varepsilon^+)$. The density of states of a harmonic oscillator with vibration frequency ν_0 is $\rho(\varepsilon_\nu) = 1/h\nu_0$, Eq. 28.3.4. Applied to our current case, the density of states of the reactive asymmetric stretch is $\rho_{rc}(\varepsilon^+) = 1/h\nu^+$. The frequency of the reaction coordinate cancels between Eq. 32.5.6 and the density of states giving the unimolecular rate constant as:¹³

$$k_a(\varepsilon^*) = \frac{1}{h} \frac{\rho^+(\varepsilon^*)}{\rho^*(\varepsilon^*)} \quad 32.5.8$$

The density of states of the activated molecule, A^* , includes all rotations and normal modes of vibration, which form a continuum at the typically high energies required to surmount the energy barrier. However, the vibrations and rotations of the critical configuration are close in energy to the zero-point. As a consequence, we cannot consider the critical configuration energy states as a continuum. The number of accessible states must be determined by explicit summation. For a given excitation energy, a range of vibrational and rotational energy states contribute: low lying ro-vibrational states contribute if the energy in the reaction coordinate is large, higher energy ro-vibrational states contribute if the energy in the reaction coordinate is small. The range of vibrational and rotational states that contribute to the reaction rate for a given ε^* is from $\varepsilon_{vr}^+ = 0$ to ε^+ . Let $N^+(\varepsilon^+)$ be the total number of vibrational and rotational states with energies from $\varepsilon_{vr}^+ = 0$ to ε^+ . The unimolecular rate constant with excitation energy ε^* is then:¹³

$$k_a(\varepsilon^*) = \frac{1}{h} \frac{N^+(\varepsilon^+)}{\rho^*(\varepsilon^*)} \quad 32.5.8$$

The critical configuration state count and the density of states of the activated molecule are tricky to calculate; computer algorithms are available to aid the calculations. More importantly, the final result is easily interpretable on the same basis as activated complex theory. We need to consider those molecular properties that enhance the number of accessible states, such as low normal mode vibrational frequencies and large rotational constants. The approach is called **RRKM** theory, named after the original developers: O. K. Rice, H. C. Ramsperger, L. S. Kassel, and R. A. Marcus. Our derivation is simplified; more general treatments are available.¹⁴⁻¹⁵

Transition state theory and classical trajectory calculations provide the foundation of theories of reaction rates in the gas phase. While not as quantitatively accurate as we would like, these approaches provide a useful perspective that we can use to picture the processes that occur upon the formation of the transition state or critical configuration. Can these models be extended into solution? Are gas phase theories useful in understanding reactions in solution?

32.6 Reaction Rates in Solution

A variety of behaviors are observed for solution phase reactions in comparison with the corresponding gas phase reactions. Solution phase reactions can be faster, the same rate, or slower than the gas phase process. The determining factor is often the polarity of the reactants or the polarity of the activated complex as compared to the reactants. Reaction dynamics in solution is a vast field. For our introduction to the field, we focus on two special cases, non-polar reactants and ionic reactants in aqueous solution.

Some Reactions are Diffusion Limited: The rate constant of many reactions in solution is equal to the diffusion coefficient of the reactants in the given solvent. This effect is especially common with non-polar reactants in aqueous solution. In Sec. 19.2 we noted that non-polar solutes are often structure makers. The entropy of the primary solvation sphere is more ordered than the bulk of the solvent. The ordered primary solvation sphere acts as a cage around the solutes. As two non-polar reactants diffuse together, the solvent cages merge. The reactants are then held in close proximity in the combined solvent cage, which allows multiple collisions to occur. The multiple collisions alleviate steric restrictions that slow reactions in the gas phase, increasing the probability of the production of products. The collision of reactants in solution and the resulting

union of the solvent cages is better called an **encounter**. The reaction rate is then given by the encounter rate, which in turn is simply given by the rate of diffusion of the reactants. For more complex cases, thermodynamic transition state theory provides a useful perspective.

Activity Coefficients in Rate Laws: Thermodynamic transition state theory is easily extended to solution dynamics. In solution, the equilibrium constant for the formation of the activated complex is expressed with activities, which in turn are given by the product of the activity coefficients and the solution concentrations:

$$K_c^\ddagger = \frac{a^\ddagger}{a_A a_B} = \frac{\gamma^\ddagger/c^\circ}{\gamma_A/c^\circ \gamma_B/c^\circ} \left(\frac{[AB^\ddagger]}{[A][B]} \right) \quad 32.6.1$$

where c° is the standard state concentration, with γ^\ddagger and $[AB^\ddagger]$ as the activity coefficient and solution concentration of the activated complex. While the equilibrium constants are written in terms of the solution activities, the rate constant expression is written in terms of concentrations. Solving Eq. 32.6.1 for the concentration ratio gives:

$$\frac{[AB^\ddagger]}{[A][B]} = K_c^\ddagger c^{0-1} \frac{\gamma_A \gamma_B}{\gamma^\ddagger} \quad 32.6.2$$

The term c^{0-1} essentially handles the units conversion to give $L \text{ mol}^{-1} \text{ s}^{-1}$. Separating out the reactive asymmetric stretch using 32.1.13° and substitution into Eq. 32.1.5 gives:

$$k_2 = \frac{kT}{h} K_c^{\ddagger'} c^{0-1} \frac{\gamma_A \gamma_B}{\gamma^\ddagger} \quad 32.6.3$$

If the activated complex is stabilized in solution relative to the reactants, then γ^\ddagger is decreased compared to γ_A or γ_B and then $\gamma_A \gamma_B / \gamma^\ddagger$ is increased. As a result the activated complex is easier to form and the rate constant is increased, Figure 32.6.1.

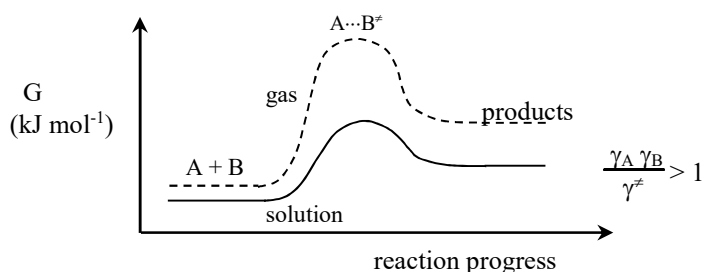


Figure 32.6.1: Stabilization of the activated complex by solvation, relative to the reactants, decreases the barrier to the formation of the activated complex, which in turn increases k_2 .

The Kinetic Salt Effect: The extension of thermodynamic transition state theory into solution is particularly easy for reactions of dilute ions. The Debye-Hückel limiting law is used to determine approximate values of the ionic activity coefficients for use in Eq. 32.6.3. For each reactant and the activated complex the Debye-Hückel activity coefficients are given as a function of the ionic strength. Combining Eqs. 19.5.30, 19.5.24, and 19.4.22 gives the activity coefficients using:

$$\ln \gamma_i = -1.171 z_i^2 I^{1/2} \quad \text{or} \quad \log \gamma_{\pm,i} = -0.509 z_i^2 I^{1/2} \quad \text{with} \quad I = \frac{1}{2} \sum z_i^2 \frac{m_i}{m^\circ} \quad 32.6.4$$

for ion i . The constants, -1.171 or -0.509 , apply to dilute aqueous solutions at 25°C . If the charges of the reactants are z_A and z_B , the activated complex has charge $z_A + z_B$:



Taking the logarithm of Eq. 32.6.3 and substituting Debye-Hückel estimates for each ion gives:

$$\begin{aligned} \log k_2 &= \log\left(\frac{kT}{h} K_c^\ddagger c^{o-1}\right) + \log \gamma_A + \log \gamma_B - \log \gamma^\ddagger \\ &= \log\left(\frac{kT}{h} K_c^\ddagger c^{o-1}\right) - 0.509 [z_A^2 + z_B^2 - (z_A + z_B)^2] I^{1/2} \\ &= \log\left(\frac{kT}{h} K_c^\ddagger c^{o-1}\right) + 0.509 (2z_A z_B) I^{1/2} \quad (\text{aqueous, } 25^\circ\text{C}) \quad 32.6.6 \end{aligned}$$

The argument of the logarithmic term is the rate constant at zero ionic strength, $k_2(I=0)$. The strong ionic strength dependence of reactions of ions is called the **kinetic salt effect** or the **primary salt effect**. The reaction rate increases or decreases with ionic strength depending on the ionic charges. The logarithm of the ratio of the rate constant to the rate constant at zero ionic strength is plotted as a function of $I^{1/2}$ in Figure 32.6.2. The slope is $0.509 (2z_A z_B)$. For example in the reaction of $\text{S}_2\text{O}_8^{2-}$ and I^- , the activated complex is more highly charged than the reactants and correspondingly has a smaller activity coefficient, giving an increase in k_2 with increasing ionic strength. For $\text{S}_2\text{O}_8^{2-}$ and I^- the activated complex is preferentially stabilized by the Coulombic forces in solution, because of the large charge of -3 , as in Figure 32.6.1. If the mechanism is unknown, the kinetic salt effect can be used to determine the charges of the reactants in the rate determining step, as $z_A z_B$.

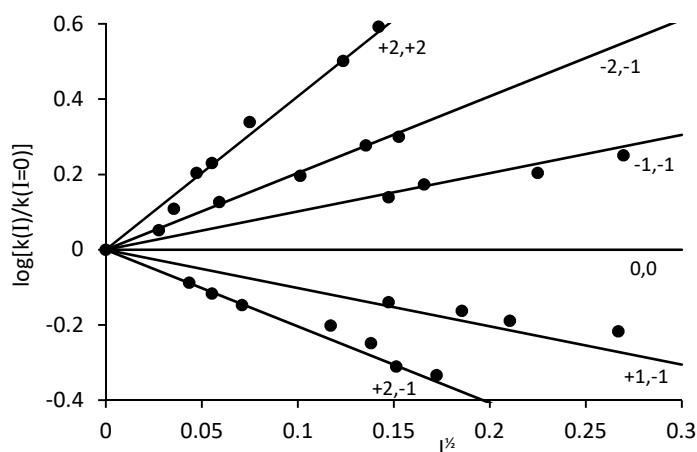
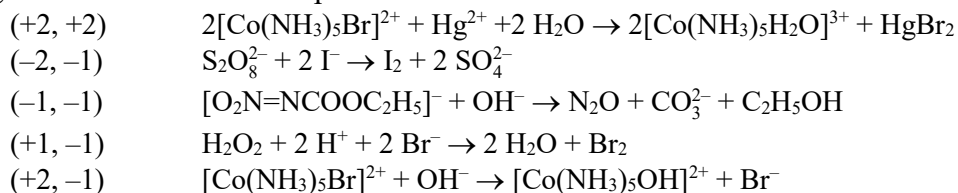


Figure 32.6.2: Kinetic salt effect. Reactions:¹⁶



32.7 Collision Theory

In the previous chapter we discussed the kinetic molecular theory approach to molecular collisions. Many extensions of basic KMT have been developed. In particular, the influences of intermolecular forces and of the translational energy demand of reactive collisions have been determined.

The Collision Cross-Section and Intermolecular Forces: Careful experiments show that collision cross-sections are functions of the collision energy. Until now, we have assumed that the collision partners act like billiard balls. If attractive and repulsive forces act between collision partners, the effective size of the collision partners depends on the relative collision energy, Figure 32.7.1.¹⁷ The collision trajectories are shown as a function of the impact parameter, b . The impact parameter is the straight-line distance between the centers of mass at closest approach. For direct, “head-on” collisions, the impact parameter is zero. For hard-core collisions the impact parameter must be less than or equal to the hard-core diameter, $b \leq d_{\text{HC}}$. Considering intermolecular forces, the collision cross-section is greater than the hard-core value for low collision energy and smaller than the hard-core value for large collision energy.¹⁸ For low collision energy the partners are pulled together so they don’t need as small an impact parameter to interact as is necessary for hard spheres. For high collision energy, the angle of deflection of the collision trajectories is decreased, showing less change than hard-core collisions. In effect, the spheres are “squishy” so they can slip by each other for impact parameters less than but close to the hard-core diameter. As a result the collision cross-section is dependent on relative collision energy, $\sigma(\epsilon_{\text{rel}})$. We have not taken this energy dependence into account in deriving the bimolecular rate constant using kinetic molecular theory, Eq. 31.3.25.

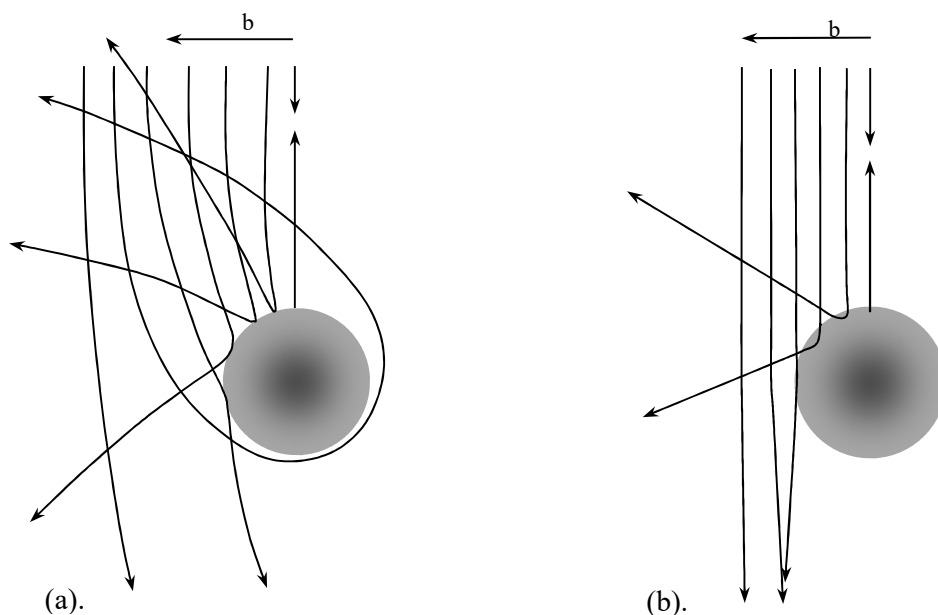


Figure 32.7.1: Collision trajectories for a Lennard-Jones 6-12 potential, Eq. 8.8.17. (a). The collision cross-section is greater than the hard-core value for low collision energy. (b). The collision cross-section is smaller than the hard-core value for large collision energy. (Adapted from Ref. 17)

Thermal Reaction Cross-Sections Include Collision Size and Reaction Probability: The bimolecular collision rate derived using kinetic molecular theory, $k_2 = \sigma_{\text{HC}} \bar{c}_{\text{rel}} (1000 \text{ L/m}^3) N_{\text{A}}$, usually greatly overestimates the value of the bimolecular rate constant. The use of the hard-core cross-section is the source of the overestimate. Because of the collision energy dependence, not all collisions have the same effective cross-section. In addition, the hard-core collision rate is the rate of all collisions, many of which do not give products. We can use Eq. 31.3.25 to calculate the **thermal reaction cross-section**, which is the effective cross-section for the production of products averaged over all collisions.¹⁹ For example for the $\text{H}_2 + \text{I}_2 \rightarrow 2 \text{HI}$ reaction, the experimental rate constant is $0.0764 \text{ L mol}^{-1} \text{ s}^{-1}$ at 700 K. From Example 31.3.2, the relative speed is 2722 m s^{-1} giving the thermal reaction cross section, $\bar{\sigma}_{\text{r}}$, as:

$$\begin{aligned} \bar{\sigma}_{\text{r}} &= \frac{k_2}{\bar{c}_{\text{rel}} (1000 \text{ L/m}^3) N_{\text{A}}} = \frac{0.0764 \text{ L mol}^{-1} \text{ s}^{-1}}{2722 \text{ m s}^{-1} (1000 \text{ L/m}^3) 6.022 \times 10^{23} \text{ mol}^{-1}} \\ &= 4.66 \times 10^{-32} \text{ m}^2 = 0.466 \text{ nm}^2 = 4.66 \times 10^{-12} \text{ \AA}^2 \end{aligned} \quad 32.7.1$$

This effective cross-section is much smaller than the molecular sizes. The corresponding interpretation is that the reaction cross-section not only expresses the physical size of the collision partners but also includes the likelihood of a reaction. The likelihood of a reaction depends on the relative collision energy. We might expect that the greater the collision energy, the greater the probability of reaction, and the greater the reaction cross-section. As a result, we once again find that the collision cross-section is a function of energy, $\sigma(\epsilon_{\text{rel}})$.

Kinetic Molecular Theory and Reactive Bimolecular Collisions: To incorporate the energy dependence of the cross-section into the theory of bimolecular collisions, we need to return to the derivation of the KMT collision rate. The bimolecular rate constant is the average of the rate of collisions with cross-section $\sigma(\epsilon_{\text{rel}})$ over the distribution of relative kinetic energy, $p(\epsilon_{\text{rel}}) d\epsilon_{\text{rel}}$:

$$k_2 = N_{\text{A}} \int_0^{\infty} \sigma(\epsilon_{\text{rel}}) c_{\text{rel}} p(\epsilon_{\text{rel}}) d\epsilon_{\text{rel}} \quad 32.7.2$$

The relative speed and kinetic energy are related by $\epsilon_{\text{rel}} = \frac{1}{2} \mu c_{\text{rel}}^2$ or $c_{\text{rel}} = (2\epsilon_{\text{rel}}/\mu)^{1/2}$. Substituting for the relative speed in the last equation gives the rate constant entirely in terms of the relative collision kinetic energy:

$$k_2 = \left(\frac{2}{\mu}\right)^{1/2} N_{\text{A}} \int_0^{\infty} \sigma(\epsilon_{\text{rel}}) \epsilon_{\text{rel}}^{1/2} p(\epsilon_{\text{rel}}) d\epsilon_{\text{rel}} \quad 32.7.3$$

Our supposition is that only collisions with relative kinetic energy exceeding a threshold, ϵ^* , are reactive. For typical reactions this threshold energy is large compared to kT and the corresponding fraction of collisions with sufficient kinetic energy is quite small, Eq. 31.4.9. As a result, the collision cross-section is zero for energies less than the threshold. As a first approximation, we assume that the cross-section is equal to the hard-core cross-section for energies higher than the threshold:

$$\sigma(\epsilon_{\text{rel}}) = 0 \quad \text{if } \epsilon_{\text{rel}} < \epsilon^* \quad \text{and} \quad \sigma(\epsilon_{\text{rel}}) = \sigma_{\text{HC}} \quad \text{if } \epsilon_{\text{rel}} \geq \epsilon^* \quad 32.7.4$$

If only collisions with relative kinetic energy above ϵ^* have a non-zero cross-section, we can change the integral limits to ϵ^* to ∞ and substitute σ_{HC} for $\sigma(\epsilon_{\text{rel}})$. Finally, the Maxwell distribution of relative kinetic energy is given by combining Eqs. 31.5.19, 31.4.3, and 32.7.3:

$$k_2 = \left(\frac{2}{\mu}\right)^{1/2} 2\pi N_A \left(\frac{1}{\pi kT}\right)^{3/2} \int_{\varepsilon^*}^{\infty} \sigma_{\text{HC}} \varepsilon_{\text{rel}} e^{-\varepsilon_{\text{rel}}/kT} d\varepsilon_{\text{rel}} \quad (\sigma_{\text{HC}} \text{ for } \varepsilon_{\text{rel}} > \varepsilon^*) \quad 32.7.5$$

Leaving the integral to the Problems and converting to molar units gives:

$$\begin{aligned} &= \sigma_{\text{HC}} \left(\frac{8}{\pi\mu}\right)^{1/2} \left(\frac{1}{kT}\right)^{3/2} (1000 \text{ L/m}^3) N_A (kT)^2 \left(1 + \frac{\varepsilon^*}{kT}\right) e^{-\varepsilon^*/kT} \\ &= \sigma_{\text{HC}} \left(\frac{8kT}{\pi\mu}\right)^{1/2} (1000 \text{ L/m}^3) N_A \left(1 + \frac{\varepsilon^*}{kT}\right) e^{-\varepsilon^*/kT} \quad (\sigma_{\text{HC}} \text{ for } \varepsilon_{\text{rel}} > \varepsilon^*) \quad 32.7.6 \end{aligned}$$

$$= \sigma_{\text{HC}} \bar{c}_{\text{rel}} (1000 \text{ L/m}^3) N_A \left(1 + \frac{\varepsilon^*}{kT}\right) e^{-\varepsilon^*/kT} \quad (\sigma_{\text{HC}} \text{ for } \varepsilon_{\text{rel}} > \varepsilon^*) \quad 32.7.7$$

For purposes of comparison with Arrhenius form, we assume the threshold energy is roughly equivalent to the activation energy. Then the term multiplying the exponential factor in Eqs. 32.7.6 and 32.7.7 is the pre-exponential factor, A:

$$\begin{aligned} A &= \sigma_{\text{HC}} \left(\frac{8kT}{\pi\mu}\right)^{1/2} (1000 \text{ L/m}^3) N_A \left(1 + \frac{\varepsilon^*}{kT}\right) \\ &= \sigma_{\text{HC}} \bar{c}_{\text{rel}} (1000 \text{ L/m}^3) N_A \left(1 + \frac{\varepsilon^*}{kT}\right) \quad (\sigma_{\text{HC}} \text{ for } \varepsilon_{\text{rel}} > \varepsilon^*) \quad 32.7.8 \end{aligned}$$

The Arrhenius pre-exponential factor is often observed to be independent of or weakly dependent on the temperature, Eq. 3.5.19. If $\varepsilon^* \gg kT$, the overall temperature dependence in Eq. 32.7.8 is $\sim T^{-1/2}$. While plausible for some reactions, this temperature dependence is not often observed. The problem is that we assumed that the cross-section of reactive collisions is constant at the hard-core value. The temperature dependence in Eq. 32.7.8 suggests that not all collisions with relative kinetic energy greater than the threshold are successful.

*Reaction Cross-Sections are a Function of Collision Energy:*²⁰ We next add the assumption that the probability of a reactive collision increases with relative kinetic energy. The threshold is the minimum relative kinetic energy that gives products; any excess beyond the threshold increases the probability of reaction. The problem is that not all collisions are direct, “head-on” collisions. Most collisions occur with non-zero impact parameter and therefore the available collision energy is less than the full collision energy. The full collision energy is $\varepsilon_{\text{rel}} = \frac{1}{2}\mu c_{\text{rel}}^2$. Consider several collisions at increasing impact parameter, Figure 32.7.2. For simplicity we assume that one molecule is stationary, within the center-of-mass reference frame, while the partner travels at the relative collision velocity \vec{v}_{rel} . The direction of the collision is given by the velocity vector of the moving molecule, Figure 32.7.2a. The magnitude of the relative velocity vector is the relative speed, c_{rel} . As the impact parameter increases, less collision energy is available, Figure 32.7.2b. If b is at the maximum value of the collision, $b = b_{\text{max}}$, essentially no collision energy is available for bond breaking and making steps. In other words, if $b = b_{\text{max}}$ the collision is a grazing collision. The collision energy is transferred at the instant of collision. A simple approximation is that the available collision energy is given by the **line-of-centers kinetic energy**, ε_{lc} . The line-of-centers is the line extending between the molecular centers at the instant of the collision. The kinetic energy along the line-of-centers is given by the speed along the line of centers: $\varepsilon_{\text{lc}} = \frac{1}{2}\mu c_{\text{lc}}^2$. The line-of-centers speed is the magnitude of the projection of \vec{v}_{rel} along the line-of-centers, Figure 32.7.2c. The line-of-centers angle, α , is also defined at the instant of the collision. Remember that in a right-triangle the cosine of the angle is the ratio of the side adjacent divided

by the hypotenuse: $\cos \alpha = c_{lc}/c_{rel}$. The speed along the line-of-centers is then a function of the collision angle:

$$c_{lc} = c_{rel} \cos \alpha \quad 32.7.9$$

where α depends on the impact parameter. For example, if $b = 0$ then $\alpha = 0^\circ$, $c_{lc} = c_{rel}$, $\epsilon_{lc} = \epsilon_{rel}$, and the full collision energy is available for bond breaking and making. If $b = b_{max}$, $\alpha = 90^\circ$ and the line-of-centers speed and collision energy are zero.

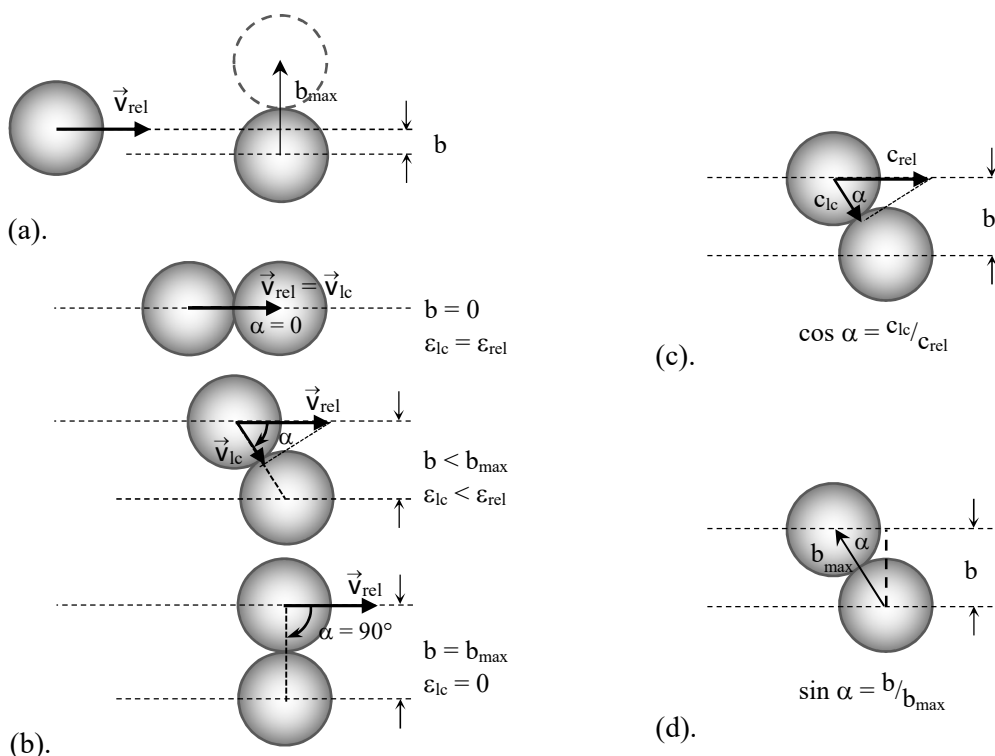


Figure 32.7.2: Line-of-centers collision energy. (a). Before the collision with impact parameter, b . The direction of the collision is determined by \vec{v}_{rel} . (b). Three different collisions. The line-of-centers kinetic energy is available at the instant of collision. (c). Geometric relationships defining the line-of centers speed, c_{lc} . (d). Geometric relationships defining the line-of centers angle, α , in terms of the impact parameter, b .

The line-of-centers angle is determined by the impact parameter, Figure 32.7.2d:

$$\sin \alpha = b/b_{max} \quad 32.7.10$$

Given that $\cos^2 \alpha = 1 - \sin^2 \alpha$ and $\epsilon_{lc} = \frac{1}{2} \mu c_{lc}^2$, the line-of-centers collision energy is:

$$\epsilon_{lc} = \frac{1}{2} \mu c_{lc}^2 = \frac{1}{2} \mu c_{rel}^2 \cos^2 \alpha = \frac{1}{2} \mu c_{rel}^2 (1 - \sin^2 \alpha) = \epsilon_{rel} (1 - b^2/b_{max}^2) \quad 32.7.11$$

Collisions occur with a statistical distribution of impact parameters. The reaction cross-section has the radius given by the average of the impact parameters of all reactive collisions. The

probability of a collision with impact parameter b is proportional to the area of an annulus of radius b and thickness db , which is: $\pi(b + db)^2 - \pi b^2 = 2\pi b db$, Figure 32.7.3. All molecules within this annulus have the same impact parameter. However, we must only count collisions that have sufficient energy to exceed the threshold; that is $\epsilon_{lc} > \epsilon^*$. The maximum impact parameter, b^* , meeting the energy threshold is given by:

$$\epsilon_{lc} = \epsilon_{rel}(1 - b^2/b_{max}^2) \geq \epsilon^* \quad \text{or} \quad b^* \leq b_{max}(1 - \epsilon^*/\epsilon_{rel})^{1/2} \quad (\epsilon_{lc} > \epsilon^*) \quad 32.7.12$$

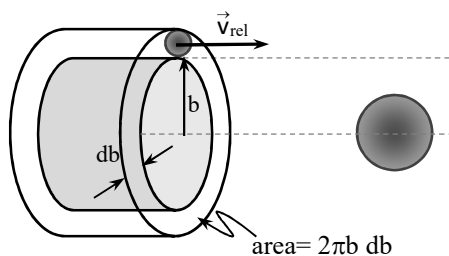


Figure 32.7.3: Large impact parameter collisions are more probable than small impact parameter collisions. Molecules within an area of an annulus of radius b and thickness db have the same impact parameter.

The probability that a collision with relative kinetic energy ϵ_{rel} and impact parameter b gives products is $P(\epsilon_{rel}, b)$. The reaction cross-section is then the integral of the reaction probability over the impact parameter:

$$\sigma(\epsilon_{rel}) = 2\pi \int_0^\infty P(\epsilon_{rel}, b) b db \quad (\epsilon_{lc} > \epsilon^*) \quad 32.7.13$$

Assuming that the reaction probability is zero for impact parameters greater than b^* allows the integral limits to be reduced to 0 to b^* . Assuming that the reaction probability is unity for every collision with the line-of-centers energy greater than the threshold, $P(\epsilon_{rel}, b) = 1$ for $\epsilon_{lc} > \epsilon^*$, gives the cross-section as:

$$\sigma(\epsilon_{rel}) = 2\pi \int_0^{b^*} b db = \pi b^{*2} \quad (\epsilon_{lc} > \epsilon^*) \quad 32.7.14$$

Substituting Eq. 32.7.12 for the maximum impact parameter gives the cross-section:

$$\sigma(\epsilon_{rel}) = \pi b_{max}^2 (1 - \epsilon^*/\epsilon_{rel}) \quad (\epsilon_{lc} > \epsilon^*) \quad 32.7.15$$

For small threshold energies this result is analogous to the hard-core result, $\sigma(\epsilon_{rel}) = \pi b_{max}^2 \cong \sigma_{HC}$. The reaction cross-section begins at zero at the threshold energy and increases to the maximum value, πb_{max}^2 , Figure 32.7.4. We can now calculate the bimolecular rate constant.

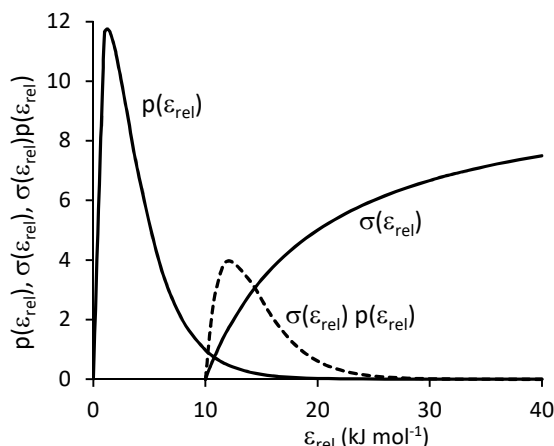


Figure 32.7.4: Maxwell distribution of kinetic energy, $p(\epsilon_{\text{rel}})$, reaction cross-section, $\sigma(\epsilon_{\text{rel}})$, and the principle contributions to the cross-section, $\sigma(\epsilon_{\text{rel}})p(\epsilon_{\text{rel}})$ (-----). This example uses $\epsilon^* = 10 \text{ kJ mol}^{-1}$, $\sigma_{\text{HC}} = 10 \text{ \AA}^2$, at 298.2 K. (The Maxwell distribution is scaled as $p(\epsilon_{\text{rel}})/10^{19}$).

Using Eqs. 32.7.5 and 32.7.15, the bimolecular rate constant is the average of $[\sigma(\epsilon_{\text{rel}}) c_{\text{rel}} N_A]$ over the Maxwell distribution. Since the reaction cross section is zero below the threshold energy, we can narrow the integration limits to ϵ^* to ∞ :

$$k_2 = \left(\frac{2}{\mu}\right)^{1/2} 2\pi N_A \left(\frac{1}{\pi kT}\right)^{3/2} \int_{\epsilon^*}^{\infty} \pi b_{\text{max}}^2 (1 - \epsilon^*/\epsilon_{\text{rel}}) \epsilon_{\text{rel}}^{1/2} e^{-\epsilon_{\text{rel}}/kT} d\epsilon_{\text{rel}} \quad (\epsilon_{\text{lc}} > \epsilon^*) \quad 32.7.16$$

Leaving the integral to the Problems and converting to molar units gives:

$$k_2 = \pi b_{\text{max}}^2 \bar{c}_{\text{rel}} (1000 \text{ L/m}^3) N_A e^{-\epsilon^*/kT} \quad (\epsilon_{\text{lc}} > \epsilon^*) \quad 32.7.17$$

The πb_{max}^2 term is analogous to the hard-core cross-section. For purposes of comparison with Arrhenius form, we assume the threshold energy is roughly equivalent to the activation energy. Then the term multiplying the exponential factor in Eq. 32.7.15 is the pre-exponential factor, A :

$$A = \pi b_{\text{max}}^2 \bar{c}_{\text{rel}} (1000 \text{ L/m}^3) N_A \quad (\epsilon_{\text{lc}} > \epsilon^*) \quad 32.7.18$$

The predicted pre-exponential factor temperature dependence is determined by \bar{c}_{rel} , which varies as $\sim T^{1/2}$. However, the Arrhenius pre-exponential factor is temperature independent. For most reactions the weak temperature dependence of the pre-exponential factor is overshadowed by the exponential term. As a result, the functional form of the pre-exponential factor is difficult to determine experimentally. Many reactions are equally well fit with temperature independent and temperature dependent pre-exponentials. However, where experimental data is available over a wide temperature range, a pre-exponential that increases with temperature is common. For example, $\text{O} + \text{H}_2 \rightarrow \text{OH} + \text{H}$ has $k_2 = 1.8 \times 10^7 T e^{-E_a/RT}$, with $E_a = 37.2 \text{ kJ mol}^{-1}$.²¹ The weak increase of A with temperature in Eq. 32.7.18 is generally more common than the form of Eq. 32.7.8.

More importantly, collision theory predictions based on Eq. 32.7.16 often overestimate reaction rates, in some cases by more than an order of magnitude. The difference between theory and experiment is often ascribed to orientation effects during the collision. For the reaction

$\text{CH}_3 + \text{HI} \rightarrow \text{CH}_4 + \text{I}$, for example, the collision geometry $\text{CH}_3 + \text{H-I}$ is more likely to produce products than $\text{CH}_3 + \text{I-H}$. To account for orientation effects, a **steric factor**, p , is introduced into Eq. 32.7.18: $A = p \pi b_{\text{max}}^2 \bar{c}_{\text{rel}} (1000 \text{ L/m}^3) N_{\text{A}}$. However, p is usually difficult to calculate from theory. Transition state theory and classical trajectory calculations are better equipped to handle steric effects than is basic collision theory. In summary, the assumption that is required to achieve agreement with experiment for many reactions is that the line-of-centers translational kinetic energy must exceed a threshold value, ϵ^* . This threshold value is related to, but not equal to the experimental activation energy.

The experimental activation energy is a thermal average over all collision conditions, including relative collisional kinetic energy, impact parameter, initial vibrational and rotational state, collision orientation, and collision timing. Quantum effects such as tunneling are also often significant. Perhaps the best definition of the activation energy is due to Tolman: the activation energy is the difference between the average energy of all reactive collisions and the average energy of all collisions.^{22,23} Approaches based on kinetic molecular theory are too coarse-grained to take internal degrees of freedom and collision timing into effect. Only classical or, even better, quantum mechanical trajectory calculations are sufficiently detailed to determine the activation energy of a reaction. However the computational complexity of averaging over all internal degrees of freedom and reaction trajectories is daunting.

32.8 Summary – Looking Back

We have barely scratched the surface of the theories of reaction dynamics. However, we have introduced three major points of view: collision theory based upon kinetic molecular theory, transition state theory based upon statistical mechanics, and classical trajectory studies based upon classical motion on quantum mechanical potential energy surfaces. These treatments will hopefully provide an adequate basis for your further study. Collision theory introduces the concepts of center of mass coordinates, energy dependent cross-sections, impact parameters, and threshold relative kinetic energy. Transition state theory introduces the statistical distribution of the available thermal kinetic energy into the reactive asymmetric stretch and internal degrees of freedom of the activated complex. Classical trajectory calculations introduce potential energy surfaces, the determination of the full reaction coordinate, vibrational and rotational state-specific reaction probabilities, and reaction timing. Trajectory calculations also introduce multiple crossing of the transition state surface.

In reflection it is interesting to note that thermodynamics provides a singular, unified view of macroscopic equilibrium. Quantum mechanics provides a singular, unified view of molecular structure and spectroscopy. However at this stage of development, reaction dynamics requires multiple points of view, because of the inherent complexity. Reaction dynamics is one of the most active areas of current research.

We have emphasized chemical reactivity and structure-function relationships throughout our study. Thermodynamics is the study of the equilibrium state. Quantum mechanics is the study of individual atoms and molecules and their interactions. Statistical mechanics is the bridge that relates molecular structure to the equilibria and rates of chemical reactions. The fundamental principle of statistical mechanics is that the most probable state is the equilibrium state. Random statistical chance determines the outcome of chemical processes. However, because of the large number of molecules involved we can focus only on the most probable distribution of energy. Through statistical mechanics, the intricate detail of the microscopic world is transformed into the equilibrium and rate constants that are needed to understand the position of equilibrium and

the approach to equilibrium. These relationships underlie all chemical phenomena. Current theory is sufficient to calculate, from first principles, the equilibrium constants of ideal gas reactions more accurately than can be determined in the laboratory. Rapid progress is being made towards the first-principles calculation of rate constants of chemical reactions and spectroscopic relaxation phenomena. Further progress is needed in solvation energetics before accurate calculations of equilibrium constants and rate constants in solution can be made.

What is this knowledge good for? All the phenomena in our physical world have a molecular basis. Solving critical challenges in day-to-day life is enabled by the careful understanding of the underlying form of nature. The perspectives gained by understanding the molecular basis of structure-function relationships inform all our research efforts. Rapid progress in the future is enabled by the careful understanding of the work of those scientists who have come before us. In every aspect, much more is known than we have presented here. The foundations of physical chemistry are well established. At the same time, much is left unknown. Many key attributes of chemical phenomena remain for you to discover.

Chapter Summary

1. The reaction coordinate is an unstable asymmetric stretch.
2. The configuration of atoms at the transition state is the activated complex, which is denoted \ddagger .
3. The effective vibrational frequency of the reactive asymmetric stretch, ν^\ddagger , is the frequency of crossing the transition state surface. Approximately, the activated complex forms products half the time with rate ν^\ddagger and returns to reactants half the time with rate ν^\ddagger .
4. The activated complex can be considered to be in equilibrium with the reactants, with equilibrium constant K_c^\ddagger :

$$K_c^\ddagger = \frac{[AB^\ddagger]}{[A][B]} \quad \text{giving} \quad k_2 = \nu^\ddagger K_c^\ddagger = \nu^\ddagger \left(\frac{RT}{P^\circ} \right) K_p^\ddagger$$

5. K_c^\ddagger is the number of accessible states of the activated complex divided by the number of accessible states of the reactants. The quantum mechanical zero-point energy shift is ΔE_0^\ddagger :

$$K_c^\ddagger = \frac{[AB^\ddagger]}{[A][B]} = \frac{q^{\ddagger\circ}/N_A}{(q_A^\circ/N_A)(q_B^\circ/N_A)} \left(\frac{RT}{P^\circ} \right) e^{-\Delta E_0^\ddagger/kT}$$

6. The reactive asymmetric stretch is separated from the partition function of the activated complex, $q^\ddagger = q_v^\ddagger q^{\ddagger\circ'}$, where $q^{\ddagger\circ'}$ includes the remaining vibrations along with translation, rotation, and electronic partition functions. Assuming the activated complex is loosely bound and unstable, $h\nu^\ddagger/kT \ll 1$ gives: $q_v^\ddagger = kT/h\nu^\ddagger$
7. The bimolecular rate constant as approximated by activated complex theory, ACT, is:

$$k_2 = \frac{kT}{h} \frac{q^{\ddagger\circ'}/N_A}{(q_A^\circ/N_A)(q_B^\circ/N_A)} \left(\frac{RT}{P^\circ} \right) e^{-\Delta E_0^\ddagger/kT}$$

8. Atom-recombination under ACT is consistent with hard-core collision theory. Assuming spherical structureless particles, the reduced mass of the collision is $\mu = (m_A + m_B)/m^\ddagger$. Associating $\sigma_{HC} = \pi R^{\ddagger 2}$, $\bar{c}_{rel} = (8kT/\pi\mu)^{1/2}$, rotational symmetry number $\sigma = 1$ for heteroatomic collisions, and adding threshold activation:

$$k_2 = \frac{\pi R^{\neq 2}}{\sigma} \left(\frac{8kT}{\pi \mu} \right)^{1/2} N_A e^{-\Delta E_0^\ddagger/kT}$$

9. ACT does not account for multiple crossings of the transition state barrier, coupling of internal degrees of freedom with the reactive asymmetric stretch, or quantum mechanical effects.

10. Thermodynamic Transition State Theory defines the Gibbs energy, enthalpy, and entropy of activation, $\Delta_r G^{\circ\ddagger}$, $\Delta_r H^{\circ\ddagger}$, and $\Delta_r S^{\circ\ddagger}$ through:

$$k_2 = \frac{kT}{h} \left(\frac{RT}{P^\circ} \right) e^{-\Delta_r G^{\circ\ddagger}/RT} = \frac{kT}{h} \left(\frac{RT}{P^\circ} \right) e^{\Delta_r S^{\circ\ddagger}/R} e^{-\Delta_r H^{\circ\ddagger}/RT}$$

11. For a bimolecular reaction, $\Delta_r H^{\circ\ddagger} = E_a - 2RT$ and $k_2 = \frac{kT}{h} \left(\frac{RT}{P^\circ} \right) e^2 e^{\Delta_r S^{\circ\ddagger}/R} e^{-E_a/RT}$

12. For a bimolecular reaction, the Arrhenius pre-exponential factor is: $A = \frac{kT}{h} \left(\frac{RT}{P^\circ} \right) e^2 e^{\Delta_r S^{\circ\ddagger}/R}$

13. For a unimolecular gas phase reaction or reactions in solution, $\Delta_r H^{\circ\ddagger} = E_a - RT$ and:

$$k_1 = \frac{kT}{h} e^{\Delta_r S^{\circ\ddagger}/R} e^{-\Delta_r H^{\circ\ddagger}/RT}$$

14. For a unimolecular gas phase reaction or reactions in solution, the linearized form is:

$$\ln\left(\frac{k_1}{T}\right) = -\frac{\Delta_r H^{\circ\ddagger}}{R} \left(\frac{1}{T}\right) + \frac{\Delta_r S^{\circ\ddagger}}{R} + \ln\left(\frac{k}{h}\right)$$

15. Bimolecular pre-exponential factors of $A = 10^{10}$ - 10^{11} L mol⁻¹ s⁻¹ give $\Delta_r S^{\circ\ddagger} \cong -80$ J K⁻¹ mol⁻¹.

16. Reactions with $\Delta_r S^{\circ\ddagger}$ more negative than -80 kJ mol⁻¹ are presumed to have a strong orientation preference.

17. Unimolecular processes are expected to have $\Delta_r S^{\circ\ddagger} \geq 0$: $AB \rightarrow (A\cdots B)^\ddagger \rightarrow A + B$

18. The transition state has one and only one imaginary normal mode frequency.

19. In classical collision dynamics the total energy of the collision is the sum of the electronic, vibrational, rotational, and relative translational kinetic energy: $\epsilon_{\text{tot}} = \epsilon_{\text{elec}} + \epsilon_v + \epsilon_r + \epsilon_{\text{rel}}$. The relative translational kinetic energy is converted by the collision into energy in the reactive asymmetric stretch.

20. The transition state barrier is the quantum barrier height, $\Delta\epsilon_b$, adjusted by the zero point energies of the reactants, ZPE_{react} , and transition state, ZPE^\ddagger . $\Delta E_0^\ddagger = \Delta\epsilon_b + ZPE^\ddagger - ZPE_{\text{react}}$

21. The transition state is a saddle-point on the quantum mechanical potential energy surface.

22. Direct transitions are typical and require times typical of a single vibration period, 10-20 fs.

23. Reactions appear to be slow because few collisions result in the formation of products, as a result of insufficient collision energy, improper orientation, or poor collision timing.

24. The energy demand of late barriers favors vibration, while early barriers favor translation.

25. The energy disposal of late barriers favors translation, while early barriers favor vibration.

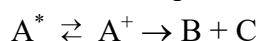
26. Reaction timing with respect to the phase of the vibrations of the reactants can have a significant effect on the reaction probability.

27. In molecular beam studies, the velocity of the reactants can be chosen using a velocity selector, which is a set of spinning disks with offset slots.

28. The molecular beam scattering angular distribution depends on the potential energy surface.

29. Short lifetime transition states give narrow angular distribution in scattering: stripping gives forward and rebound gives backward scattering in the center of mass reference frame.

30. Supersonic expansion sources produce low molecular beam temperatures with most molecules in low lying rotational J-states within the zero-point vibrational level.
31. All chemical reactions that require bond scission result from the break-down of the Born-Oppenheimer approximation: the electronic energy is coupled to the nuclear motion.
32. Non-adiabatic curve-crossing joins reactant and product potential energy surfaces.
33. The probability of unimolecular reaction depends on the excitation energy.
34. In unimolecular processes, the activated complex is called the critical configuration, A^\ddagger :



35. The unimolecular rate constant with excitation energy ε^* is: $k_a(\varepsilon^*) = \nu^\ddagger \frac{\rho^\ddagger(\varepsilon^\ddagger)}{\rho^*(\varepsilon^*)}$

where the excess energy in vibration, rotation, and the reaction coordinate available to the critical configuration is $\varepsilon^\ddagger = \varepsilon^* - \Delta E_0^\ddagger$ with ΔE_0^\ddagger the quantum mechanical energy barrier.

36. The density of states of the critical configuration $\rho^\ddagger(\varepsilon^\ddagger)$ is the product of the density of states of the reactive asymmetric stretch, $\rho_{\text{rc}}(\varepsilon^\ddagger)$, and the density of states of the remaining rotational and vibrational degrees of freedom, $\rho^+(\varepsilon^\ddagger)$. The density of states of the activated molecule, $\rho^*(\varepsilon^*)$, includes all rotations and normal modes of vibration, which typically form a continuum.
36. If $N^+(\varepsilon^\ddagger)$ is the total number of vibrational and rotational states of the critical configuration with vibrational and rotational energies from $\varepsilon_{\text{vr}}^\ddagger = 0$ to ε^\ddagger , the RRKM rate constant is:

$$k_a(\varepsilon^*) = \frac{1}{h} \frac{N^+(\varepsilon^\ddagger)}{\rho^*(\varepsilon^*)}$$

37. The rate constant of many reactions in solution with non-polar reactants is equal to the diffusion coefficient of the reactants in the given solvent. In an encounter, the collision of reactants in solution combines the solvent cages, which allows multiple collisions.
38. The ACT bimolecular rate constant in solution, with γ_A and γ_B the activity coefficients of the reactants and γ^\ddagger of the activated complex, is based on the equilibrium ratio:

$$\frac{[AB^\ddagger]}{[A][B]} = K_c^\ddagger c^{0-1} \frac{\gamma_A \gamma_B}{\gamma^\ddagger} \quad \text{giving} \quad k_2 = \frac{kT}{h} K_c^\ddagger c^{0-1} \frac{\gamma_A \gamma_B}{\gamma^\ddagger}$$

The term $c^{0-1} = 1/c^0$, with standard state $c^0 = 1 \text{ mol L}^{-1}$, converts the units of k_2 to $\text{L mol}^{-1} \text{ s}^{-1}$.

39. The kinetic salt effect is based on ACT with ionic reactants and transition state using Debye-Hückel activity coefficients, which in aqueous solution at 25° gives:

$$\log k_2 = \log \left(\frac{kT}{h} K_c^\ddagger c^{0-1} \right) + 0.509 (2Z_A Z_B) I^{1/2} \quad \text{with} \quad k_2(I=0) = \frac{kT}{h} K_c^\ddagger c^{0-1}$$

40. The impact parameter, b , is the straight-line distance between reactant's centers of mass at closest approach. Hard-core collisions have $b \leq d_{\text{HC}}$, with d_{HC} the hard-core diameter.
41. For low collision energy, attraction between collision partners allows larger b to interact, compared to hard spheres. For high collision energy, the angle of deflection of the collision trajectories is decreased compared to hard-core collisions.
42. As a result, the collision cross-section is dependent on relative collision energy, $\sigma(\varepsilon_{\text{rel}})$.
43. Thermal reaction cross-sections account for collision cross-section and reaction probability:

$$\bar{\sigma}_r = \frac{k_2}{\bar{c}_{\text{rel}} (1000 \text{ L/m}^3) N_A}$$

44. Bimolecular rate constants average the rate of collisions with cross-section $\sigma(\epsilon_{\text{rel}})$ over the distribution of relative kinetic energy, $p(\epsilon_{\text{rel}}) d\epsilon_{\text{rel}}$, with relative kinetic energy $\epsilon_{\text{rel}} = \frac{1}{2}\mu c_{\text{rel}}^2$:

$$k_2 = N_A \int_0^\infty \sigma(\epsilon_{\text{rel}}) c_{\text{rel}} p(\epsilon_{\text{rel}}) d\epsilon_{\text{rel}} = \left(\frac{2}{\mu}\right)^{1/2} N_A \int_0^\infty \sigma(\epsilon_{\text{rel}}) \epsilon_{\text{rel}}^{1/2} p(\epsilon_{\text{rel}}) d\epsilon_{\text{rel}}$$

45. Assuming $\sigma(\epsilon_{\text{rel}}) = \sigma_{\text{HC}}$ for energies higher than the threshold for reaction, ϵ^* :

$$k_2 = \left(\frac{2}{\mu}\right)^{1/2} 2\pi N_A \left(\frac{1}{\pi kT}\right)^{3/2} \int_{\epsilon^*}^\infty \sigma_{\text{HC}} \epsilon_{\text{rel}} e^{-\epsilon_{\text{rel}}/kT} d\epsilon_{\text{rel}} = \sigma_{\text{HC}} \bar{c}_{\text{rel}} (1000 \text{ L/m}^3) N_A \left(1 + \frac{\epsilon^*}{kT}\right) e^{-\epsilon^*/kT}$$

46. Assuming $\epsilon^* \cong E_a$ the Arrhenius pre-exponential factor has temperature dependence $\sim T^{-1/2}$:

$$A = \sigma_{\text{HC}} \left(\frac{8kT}{\pi\mu}\right)^{1/2} (1000 \text{ L/m}^3) N_A \left(1 + \frac{\epsilon^*}{kT}\right) = \sigma_{\text{HC}} \bar{c}_{\text{rel}} (1000 \text{ L/m}^3) N_A \left(1 + \frac{\epsilon^*}{kT}\right)$$

47. Assuming the probability of a reactive collision increases with relative kinetic energy, the maximum impact parameter, b^* , that meets the energy threshold, ϵ^* , is:

$$b^* \leq b_{\text{max}}(1 - \epsilon^*/\epsilon_{\text{rel}})^{1/2} \quad \text{giving the cross-section} \quad \sigma(\epsilon_{\text{rel}}) = \pi b_{\text{max}}^2(1 - \epsilon^*/\epsilon_{\text{rel}})$$

with b_{max} the maximum impact parameter for collision. Grazing collisions occur at $b = b_{\text{max}}$.

48. Assuming the reactive cross-section is dependent on relative kinetic energy with a threshold energy, the bimolecular rate constant is: $k_2 = \pi b_{\text{max}}^2 \bar{c}_{\text{rel}} (1000 \text{ L/m}^3) N_A e^{-\epsilon^*/kT}$

49. Assuming variable $\sigma(\epsilon_{\text{rel}})$ and $\epsilon^* \cong E_a$ the Arrhenius pre-exponential factor varies as $\sim T^{1/2}$:

$$A = \pi b_{\text{max}}^2 \bar{c}_{\text{rel}} (1000 \text{ L/m}^3) N_A$$

50. Addition of a steric factor, p , accounts for orientation effects: $A = p \pi b_{\text{max}}^2 \bar{c}_{\text{rel}} (1000 \text{ L/m}^3) N_A$

51. E_a is the difference between the average energy of all reactive collisions and the average energy of all collisions (Tolman).

Literature Cited:

1. H. S. Johnston, H. J. Crosby, "Kinetics of the Fast Gas Phase Reaction between Ozone and Nitric Oxide," *J. Chem Phys.*, **1954**, 22, 689-692.
2. H. S. Johnston, W. A. Bonner, D. J. Wilson, "Carbon Isotope Effect during Oxidation of Carbon Monoxide with Nitrogen Dioxide," *J. Chem. Phys.*, **1957**, 26, 1002-1006.
3. G. Porter, F. J. Wright, "Studies of free radical reactivity by the methods of flash photolysis. The photochemical reaction between chlorine and oxygen," *Discuss. Faraday Soc.*, **1953**, 14, 23-24.
4. H. S. Johnston, *Gas Phase Reaction Rate Theory*, Ronald Press, New York, NY, 1966. pp. 122-131.
5. A. A. Westenberg, N. de Haas, "Atom-Molecule Kinetics Using ESR Detection. III> Results for $\text{O} + \text{D}_2 \rightarrow \text{OD} + \text{D}$ and Theoretical Comparison with $\text{O} + \text{H}_2 \rightarrow \text{OH} + \text{H}$," *J. Chem. Phys.*, **1967**, 47(10), 4241-4246.
6. S. P. Walsh, A. F. Wagner, T. H. Dunning, Jr., G. C. Schatz, "Theoretical studies of the $\text{O} + \text{H}_2$ reaction," *J. Chem. Phys.*, **1980**, 72(4), 2894-2896.
7. S. P. Walch, T. H. Dunning, Jr., R. C. Raffennetti, "A theoretical study of the potential energy surface for $\text{O}(^3\text{P}) + \text{H}_2$," *J. Chem. Phys.*, **1980**, 72(1), 406-415.
8. H. Furue, P. D. Pacey, "Effective Bending Frequencies, Energies, and Tunneling Parameters of Transition States from Thermal Rate Data and Semiempirical Internuclear Distances: DHH, HDD, OHH, ODD," *J. Phys. Chem.*, **1987**, 91, 4132-4137.
9. R. S. Berry, S. A. Rice, J. Ross, *Physical Chemistry*, 2nd. Ed., Oxford Univ. Press, New York, NY, 2000. Table 30.1, p. 918.

10. R. Car, M. Parrinello, "Unified approach for molecular dynamics and density-functional theory," *Phys. Rev. Letters*, **1985**, 55(22), 2471-2474
11. M. Iannuzzi, A. Laio, M. Parrinello, "Efficient exploration of reactive potential energy surfaces using Car-Parrinello molecular dynamics," *Phys. Rev. Letters*, **2003**, 90(23), 238302:1-4
12. R. D. Levine, *Molecular Reaction Dynamics*, Cambridge Univ. Press, Cambridge, UK, 2005.
13. P. L. Houston, *Chemical Kinetics and Reaction Dynamics*, McGraw Hill, New York, NY, 2001; reprinted by Dover, Mineola, NY, 2006. Sec. 3.3, pp. 231-239.
14. P. J. Robinson, K. A. Holbrook, *Unimolecular Reactions*, Wiley-Interscience, London, UK, 1972.
15. W. C. Gardiner, *Rates and Mechanisms of Chemical Reactions*, W. A. Benjamin, New York, NY, 1969. Sec. 5-2c, pp. 125-133.
16. R. Livingston, "An Introduction to Chemical Catalysis in Homogeneous Systems," *J. Chem. Ed.*, **1930**, 7(12), 2887-2903.
17. W. Kauzmann, *Thermal Properties of Matter Vol. I: Kinetic Theory of Gases*, Benjamin, New York, NY, 1966. Fig. 5-12.
18. J. O. Hirschfelder, C. F. Curtiss, R. B. Bird, *Molecular Theory of Gases and Liquids*, Wiley, New York, NY, 1954. pp. 553-561.
19. J. S. Winn, *Physical Chemistry*, Harper Collins, New York, NY, 1995, Sec. 27.2 pp. 1049-1052.
20. P. L. Houston, *Chemical Kinetics and Reaction Dynamics*, McGraw Hill, New York, NY, 2001; reprinted by Dover, Mineola, NY, 2006. Sec. 3.3, pp. 95-99.
21. G. Dixon-Lewis, D. J. Williams, *Comprehensive Chemical Kinetics, Vol. 17*, Elsevier, Amsterdam, Netherlands, 1977. Chapt. 1.
22. R. C. Tolman, "Statistical Mechanics Applied To Chemical Kinetics," *J. Am. Chem. Soc.*, **1920**, 42, 2506-2528.
23. D. G. Truhlar, "Interpretation of the activation energy," *J. Chem. Ed.*, **1978**, 55, 309.

Further Reading:

Intermolecular Forces

W. Kauzmann, *Thermal Properties of Matter Vol. I: Kinetic Theory of Gases*, Benjamin, New York, NY, 1966.

Reaction Dynamics

P. L. Houston, *Chemical Kinetics and Reaction Dynamics*, McGraw Hill, New York, NY, 2001; reprinted by Dover, Mineola, NY, 2006.

J. W. Moore, R. G. Pearson, *Kinetics and Mechanism, 3rd Ed.*, Wiley, New York, NY, 1981.

R. D. Levine, *Molecular Reaction Dynamics*, Cambridge Univ. Press, Cambridge, UK, 2005.

R. D. Levine, R. B. Bernstein, *Molecular Reaction Dynamics and Chemical Reactivity*, Oxford Univ. Press, New York, NY, 1987.

J. I. Steinfeld, J. S. Francisco, W. L. Hase, *Chemical Kinetics and Dynamics*, Prentice Hall, Englewood Cliff, NJ, 1989.

W. C. Gardiner, *Rates and Mechanisms of Chemical Reactions*, W. A. Benjamin, New York, NY, 1969.

Classical Trajectory – Molecular Dynamics

D. C. Rapaport, *The art of molecular dynamics simulation*, Cambridge Univ. Press, Cambridge, UK, 1995.

J. M. Haile, *Molecular Dynamics Simulation: Elementary Methods*, Wiley, New York, NY, 1992.

Nature of the Transition State

P. R. Brooks, "Spectroscopy of Transition Region Species," *Chem. Rev.*, **1988**, 88, 407-428.

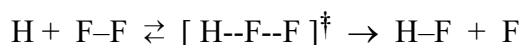
D. M. Neumark, "Transition State Spectroscopy of Bimolecular Chemical Reactions," *Ann. Rev. Phys. Chem.*, **1992**, 43, 153-176.

Chapter 32 Reaction Dynamics Problems

1. One possible geometry of the activated complex for the $2 \text{ClO} \rightarrow \text{Cl}_2 + \text{O}_2$ reaction is shown in Table 32.1.1. Is this square geometry consistent with the expectation that the reaction coordinate is an unstable asymmetric stretch?

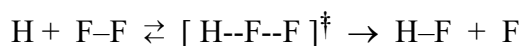
2. The lifetime of the transition state is typically on the order of a single vibration period. Calculate the period of a vibration of wave number 500 cm^{-1} .

3. Use Activated Complex Theory to discuss the reaction:



- (a). Do the translational partition functions favor or hinder the rate of the reaction? Why?
 (b). Do the rotational partition functions favor or hinder the rate of the reaction? Why?

4. Use Activated Complex Theory to discuss the reaction:

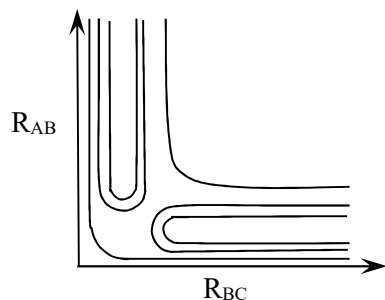


Consider the shift in reaction rate, faster or slower, after making the following changes. (a). The bond length of F_2 is increased. (b). F_2 is changed from a homonuclear to a heteronuclear diatomic. (c). The symmetric stretch force constant of the activated complex is increased. (d). The bond dissociation energy of F_2 is increased. (e). The ^1H -atom is changed to deuterium, ^2H , considering translation only. [In reality changing just one molecular parameter is impossible, bond strength changes have multiple effects. However, for the purposes of this exercise assume that the given change is done without changes in other parameters.]

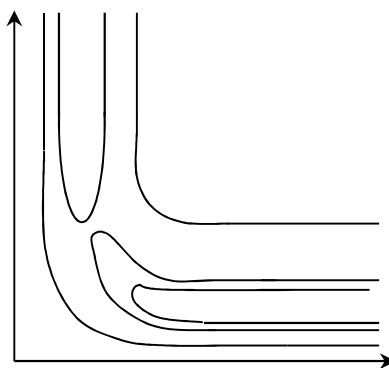
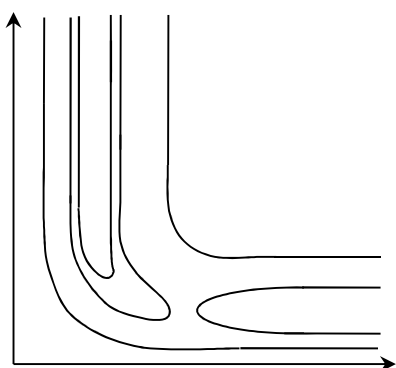
5. The pre-exponential factor for the reaction $\text{CH}_3\text{Br} + \text{Cl}^- \rightarrow \text{CH}_3\text{Cl} + \text{Br}^-$ in acetone solution is $2.0 \times 10^9 \text{ L mol}^{-1} \text{ s}^{-1}$ and its activation energy is 65.7 kJ mol^{-1} . What are the Gibbs energy, entropy, and enthalpy of activation at 298 K ?

6. In the derivation of the Eyring equation, Eq. 32.1.21°, what is the source of the kT/h term?

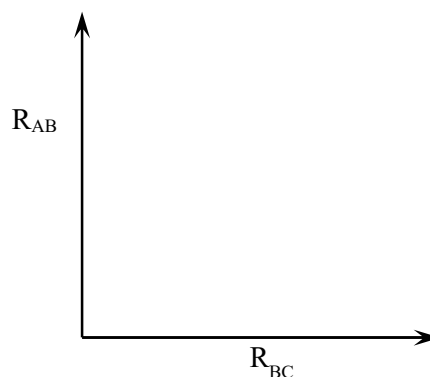
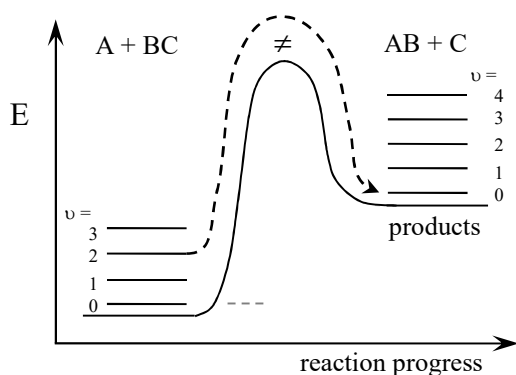
7. Draw the trajectory, on the potential energy surface below, of a reactive atom-diatom collision that experiences multiple crossings and produces a product in a highly excited vibrational state. Label the side of the graph that corresponds to the reactants and specify the corresponding reaction, choosing from either $\text{A} + \text{B}-\text{C} \rightarrow \text{A}-\text{B} + \text{C}$ or $\text{A}-\text{B} + \text{C} \rightarrow \text{A} + \text{B}-\text{C}$.



8. Consider the exothermic gas phase reaction: $\text{O}(^3\text{P}) + \text{CS} \rightarrow \text{CO} + \text{S}(^3\text{P})$. Is the reaction likely to have an early or late barrier? Does translational or vibrational energy in the collision favor the formation of products? Choose the corresponding energy surface, below. Label the axes with either R_{OC} or R_{CS} . Label the reactant and product valleys. Draw an example of a trajectory that has the favorable combination of translational and vibrational energy for the collision. (You will use only one of the surfaces)

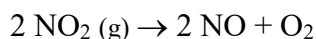


9. The reaction profile of an atom-diatom collision is shown below, including the vibrational levels. Draw a corresponding trajectory for the collision. Label the reactant and product sides.



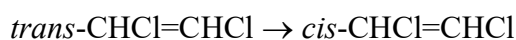
10. Use collision theory to calculate the theoretical value of the bimolecular rate constant of the reaction $\text{H}_2(\text{g}) + \text{I}_2(\text{g}) \rightarrow 2 \text{HI}(\text{g})$ at 650 K. The collision cross-section is 0.36 nm^2 , the reduced mass is $3.32 \times 10^{-27} \text{ kg}$, and the activation energy is $171. \text{ kJ mol}^{-1}$

11. (a). Find the activation enthalpy, entropy, and Gibbs energy of the reaction:



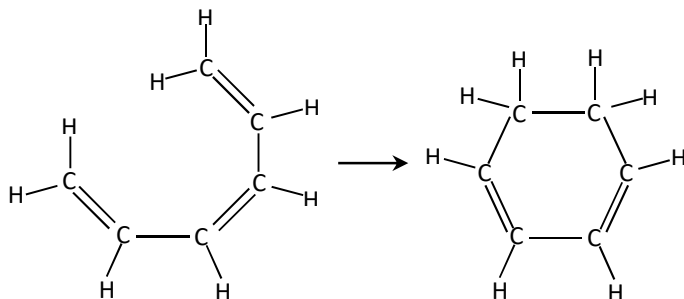
at 600.0 K. The Arrhenius pre-exponential factor is $3.06 \times 10^{12} \text{ s}^{-1}$. The activation energy is $110.9 \text{ kJ mol}^{-1}$. (b). The reaction does not necessarily proceed by a single step mechanism. Is the activation entropy consistent with a bimolecular transition state for the rate limiting step?

12. Find the activation enthalpy, entropy, and Gibbs energy of the isomerization:



at 800.0 K. The Arrhenius pre-exponential factor is $5.0 \times 10^{12} \text{ s}^{-1}$. The activation energy is 27.8 kJ mol^{-1} :

13. The reaction: *cis*-1,3,5-hexatriene \rightarrow 1,3-cyclohexadiene has an activation enthalpy of $121.5 \text{ kJ mol}^{-1}$ and an entropy of activation of $-30.4 \text{ J K}^{-1} \text{ mol}^{-1}$. Comment on the ease of formation of the transition state.



14. The rate constant of an aqueous ionic reaction with $z_A = 2$ and $z_B = -1$ at zero ionic strength is $k_{(I=0)}$. Calculate the ratio of the rate constant of the reaction done in 0.1 M NaCl, k , to the rate constant at zero ionic strength: $k/k_{(I=0)}$ at 298 K.

15. Use Eq. 32.7.13 to prove that the hard-core collision cross section is $\sigma_{\text{HC}} = \pi d_{\text{HC}}^2$, where d_{HC} is the hard-core collision diameter.

16. Determine if the following statements are true or false. If the statement is false, describe the changes that are necessary to make the statement true, if possible. If the statement is true but too restrictive, give the more general statement.

- In atom-diatom collisions, $A + BC \rightarrow AB + C$, the reaction coordinate is an unstable asymmetric stretch.
- Once the transition state surface is crossed, the activated complex does not return to reactants.
- Activated Complex Theory assumes a Boltzmann distribution among vibrations and rotations in the reactants and the activated complex.
- Excluding the reactive asymmetric stretch, the vibrations and rotations of the activated complex do not have an effect on the reaction rate.

- (e). Reactions are more likely with excess energy in translation rather than vibration.
- (f). Exothermic reactions are more likely to give products in excited vibrational states than endothermic reactions.
- (g). The common existence of chemical reactions that are much slower than the corresponding kinetic molecular theory hard-core collision rate is evidence of long-lived transition states.
- (h). In the RRKM theory of unimolecular processes, the vibrational and rotational states of the reactants are treated as a continuum while the vibrational and rotational states of the critical configuration are treated as discrete and countable.
- (i). In the RRKM theory of unimolecular processes, the critical configuration never returns to the activated reactant.
- (j). Non-adiabatic transitions occur by avoided curve crossing.
- (k). The Born-Oppenheimer approximation is valid for the progression of the transition state to give products.

- (l). Experimental reaction cross-sections are never larger than the hard-core collision cross-sections, although the experimental reaction cross-sections is often smaller than the hard-core collision cross-section.
- (m). In collision theory, the line of centers velocity and kinetic energy increase with decreasing impact parameter.
- (n). In collision theory, the reaction cross section is independent of the collision relative kinetic energy.
- (o). In solution, equilibrium constants are functions of the activities of the reactants and products, rather than the concentrations. Reaction rates are functions of the solution concentrations, and not the activities.